A North American Hourly Assimilation and Model Forecast Cycle: The Rapid Refresh

STANLEY G. BENJAMIN, STEPHEN S. WEYGANDT, JOHN M. BROWN, MING HU,*
CURTIS R. ALEXANDER,* TATIANA G. SMIRNOVA,* JOSEPH B. OLSON,* ERIC P. JAMES,*
DAVID C. DOWELL, GEORG A. GRELL, HAIDAO LIN,+ STEVEN E. PECKHAM,*
TRACY LORRAINE SMITH,+ WILLIAM R. MONINGER,* AND JAYMES S. KENYON*

NOAA/Earth System Research Laboratory, Boulder, Colorado

GEOFFREY S. MANIKIN

NOAA/NWS/NCEP/Environmental Modeling Center, College Park, Maryland

(Manuscript received 8 July 2015, in final form 8 December 2015)

ABSTRACT

The Rapid Refresh (RAP), an hourly updated assimilation and model forecast system, replaced the Rapid Update Cycle (RUC) as an operational regional analysis and forecast system among the suite of models at the NOAA/National Centers for Environmental Prediction (NCEP) in 2012. The need for an effective hourly updated assimilation and modeling system for the United States for situational awareness and related decision-making has continued to increase for various applications including aviation (and transportation in general), severe weather, and energy. The RAP is distinct from the previous RUC in three primary aspects: a larger geographical domain (covering North America), use of the community-based Advanced Research version of the Weather Research and Forecasting (WRF) Model (ARW) replacing the RUC forecast model, and use of the Gridpoint Statistical Interpolation analysis system (GSI) instead of the RUC three-dimensional variational data assimilation (3DVar). As part of the RAP development, modifications have been made to the community ARW model (especially in model physics) and GSI assimilation systems, some based on previous model and assimilation design innovations developed initially with the RUC. Upper-air comparison is included for forecast verification against both rawinsondes and aircraft reports, the latter allowing hourly verification. In general, the RAP produces superior forecasts to those from the RUC, and its skill has continued to increase from 2012 up to RAP version 3 as of 2015. In addition, the RAP can improve on persistence forecasts for the 1–3-h forecast range for surface, upper-air, and ceiling forecasts.

1. Introduction

In this paper, we describe the latest version of the Rapid Refresh assimilation/model system, which provides a critical component of NOAA weather guidance focusing on situational awareness and short-range forecasting.

Environmental situational awareness can be defined [e.g., Jeannot (2000) for air-traffic management] as having a synthesis of all available observations describing current environmental conditions to allow improved decision-making. Weather information is a key component of environmental situational awareness, and an analysis of current weather conditions and a short-range weather forecast are both critical components. The time scales for decision-making lead time and changes to environmental conditions both define the time period over which the term ''situational awareness'' may be applied. Broadly, improved situational awareness based on the latest observations improves the outcome and reduces risks for subsequent decisions.

Weather situational awareness for aviation and severe weather watches and warnings are obvious short-range forecast needs (defined here as from a few minutes

* Additional affiliation: Cooperative Institute for Research in Environmental Sciences, University of Colorado Boulder, Boulder, Colorado.

+ Additional affiliation: Cooperative Institute for Research in the Atmosphere, Colorado State University, Fort Collins, Colorado.

Corresponding author address: Stanley G. Benjamin, NOAA/ESRL, R/GSD1, 325 Broadway, Boulder, CO 80305-3328.
E-mail: stan.benjamin@noaa.gov

DOI: 10.1175/MWR-D-15-0242.1

TABLE 1. History of rapidly updated model and assimilation systems at NCEP as of late 2015.

Model and assimilation system	Horizontal grid spacing (km)	No. of vertical levels	Assimilation frequency (h)	Implementation (month/year)		Geographical domain
				NCEP	ESRL	
RUC1	60	25	3	1994		CONUS
RUC2	40	40	1	4/1998		CONUS
RUC20	20	50	1	2/2002		CONUS
RUC13	13	50	1	5/2005		CONUS
Rapid Refresh	13	51	1	5/2012	2010	North America
Rapid Refresh v2	13	51	1	2/2014	1/2013	North America
Rapid Refresh v3	13	51	1	Estimated spring 2016	1/2015	North America
HRRR	3	51	1	9/2014	2010	CONUS
HRRR v2	3	51	1	Estimated spring 2016	4/2015	CONUS

up to approximately 12-h duration), but other sectors such as hydrology and energy also have weather situational-awareness requirements. Each of these sectors requires further improvements in frequently updated, short-range NWP forecasts especially for rapidly changing weather conditions. Increasing use of automated decision-making algorithms in each of these sectors allows specific application of such frequently refreshed forecast data (Mass 2012).

In response to these requirements, in 1998, the U.S. National Oceanic and Atmospheric Administration (NOAA) introduced an operational hourly updated numerical weather prediction system [Rapid Update Cycle (RUC); Benjamin et al. (2004a,c)], the first hourly updated NWP system implemented at any operational center in the world. The hourly assimilation frequency, with the latest hourly observations used in the RUC, allowed it to serve as an initial U.S. weather situational-awareness model (Table 1).

With the growing need for increased accuracy in frequently updated, short-range weather guidance, a next-generation hourly updated assimilation and model forecast cycle, the Rapid Refresh (RAP), was developed and introduced into the operational model suite at the NOAA/National Centers for Environmental Prediction (NCEP) in May 2012, replacing

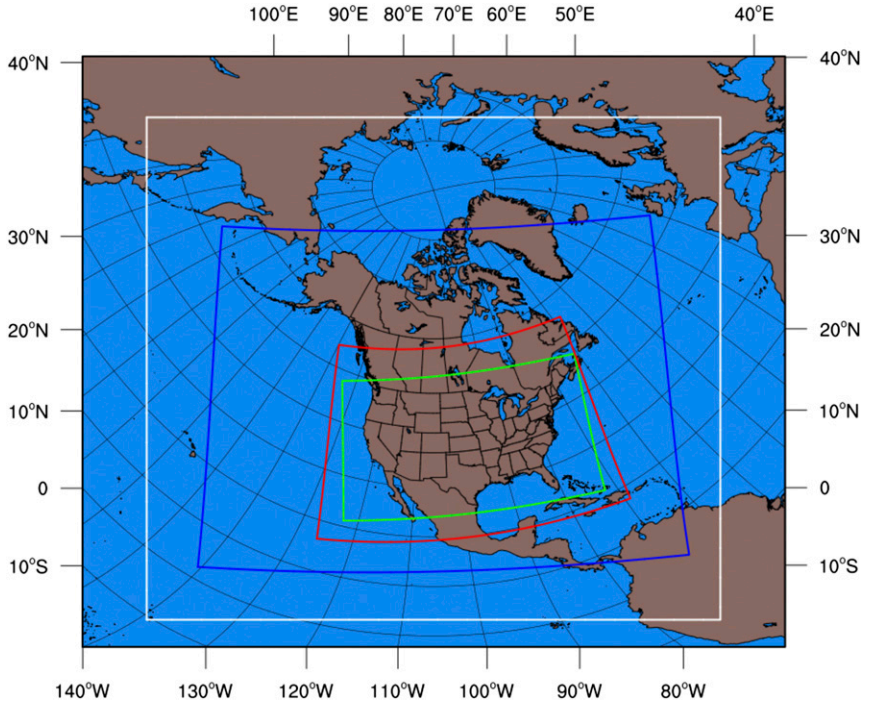

FIG. 1. Horizontal domains for the HRRR (green), RUC (red), RAPv1 and RAPv2 (blue), and expanded domain of the RAPv3 (white).

TABLE 2. Characteristics of the RAP model and assimilation system (for three versions) at NCEP compared to that for the RUC (running operationally at NCEP until 2012).

Model	Domain	Grid points	Grid spacing (km)	Vertical levels	Vertical coordinate	Pressure top (hPa)	Lateral boundary conditions
RUC	CONUS	451 × 337	13	50	Sigma/isentropic	~50	NAM
RAP	North America	758 × 567	13	51	Sigma	10	GFS
RAPv2	North America	758 × 567	13	51	Sigma	10	GFS
RAPv3	Enlarged North America	954 × 835	13	51	Sigma	10	GFS

Model	Assimilation	DFI	Cloud analysis	Microphysics	WRF version	Radiation LW/SW	Cumulus parameterization	PBL	LSM
RUC	RUC–3DVar	Yes with radar reflectivity	Yes	Thompson et al. (2004)	—	RRTM/ Dudhia	Grell–Devenyi	Burk–Thompson	RUC 2003 6 level
RAP	GSI–3DVar with radiances	Yes with radar reflectivity	Yes	Thompson et al. (2008) with enhancements	v3.2.1+	RRTM/ Goddard	Grell-3D	MYJ	RUC 2010 6 level
RAP v2	GSI with hybrid ensemble–variational (0.5/0.5) assimilation	Yes with radar reflectivity	Yes	As above, with minor adjustments	v3.4.1+	RRTM/ Goddard	Grell-3D	MYNN	RUC 2014 9 level
RAP v3	GSI hybrid ensemble–variational (0.75/0.25) assimilation	Yes with radar reflectivity and lightning	Yes	Thompson and Eidhammer (2014)	v3.6+	RRTMG	Grell and Freitas (2014)	MYNN 2015	RUC 2015 9 level

the previous RUC (Table 1). A second version of the RAP with further advances in data assimilation and model design was implemented at NOAA/NCEP in February 2014, and a third version is planned for early 2016. The RAP differs from the RUC primarily in three aspects: model component, assimilation component, and horizontal domain. Moreover, the RAP was designed to use community-based modeling and assimilation components as its foundation while incorporating unique assimilation and modeling techniques found to be beneficial specifically for short-range forecasts.

For data assimilation, the RAP uses the NOAA Gridpoint Statistical Interpolation analysis system (GSI) (Wu et al. 2002; Whitaker et al. 2008; Kleist et al. 2009) including RAP-specific enhancements designed for hourly assimilation of radar reflectivity and observations related to the boundary layer, consistent with surface, cloud, and precipitation processes (section 2). The RAP also uses a version of the Weather Research and Forecasting (WRF) community regional model (Skamarock et al. 2008; Klemp et al. 2008) capable of nonhydrostatic applications (section 3). Finally, the Rapid Refresh uses the NCEP Unified Post Processor (UPP), also used for other NCEP NWP models, with some new diagnostics added for precipitation type based on fallout of liquid and ice hydrometeor species explicitly predicted in RAP and High-Resolution Rapid Refresh (HRRR) (e.g., Benjamin et al. 2016). The horizontal domain for the RAP (versions 1 and 2) is about 3.5 times larger than that used for the RUC, covering Alaska, the Caribbean Sea, and virtually all of North America (Fig. 1). The horizontal domain has been expanded even further in version 3 of the RAP (RAPv3; Fig. 1) so that it matches the domain of the North American Mesoscale Forecast System (NAM; Janjić and Gall 2012). With this domain change from that of the RUC, the Rapid Refresh is able to provide hourly updated NWP guidance out to 18 h and situational-awareness analyses over all of North America.

A convection-allowing, 3-km hourly updated model over the lower 48 United States also including assimilation of radar reflectivity, HRRR (Smith et al. 2008) is nested within the RAP domain and strongly dependent upon RAP data assimilation. The 3-km HRRR uses the same physical parameterization configuration described here for the RAP except for no parameterization of deep convection. A history of the NOAA hourly updated models—the RUC, RAP, and HRRR and their implementations at NCEP since 1994—is shown in Table 1. A summary of model and assimilation differences between the RUC and RAP is provided in Table 2, and

TABLE 3. Analysis variables in RAPv3 and analysis method used for each variable.

Updated variables in GSI/RAP assimilation	Analysis method
	Atmospheric variables (3D)
P—pressure	GSI hybrid ensemble–variational analysis
T_v—virtual temperature	GSI hybrid ensemble–variational analysis
u, v—horizontal wind components	GSI hybrid ensemble–variational analysis
q_v—water-vapor mixing ratio	GSI hybrid ensemble–variational analysis
q*—hydrometeor mixing ratios (cloud water, ice, rainwater, snow, graupel)	Nonvariational hydrometeor analysis with GOES cloud-top data, METAR cloud data, radar reflectivity
N*—number concentrations for cloud droplets, rain drops, and ice particles	Adjustment based on q* modifications
	Land surface variables
T_{soil}—soil temperature (3D)	Adjustment using near-surface temperature and moisture analysis increment
η—volumetric soil moisture (3D)	Same as above
SWE—snow water equivalent	Same as above
Snow temperature (over two levels)	Same as above
Canopy water	Cycled but not modified in analysis

these differences are described in more detail in the following sections.

Each modification to the model or assimilation during NWP system development begins as a scientific hypothesis about how the model represents the actual atmosphere or how observations can be used to correct the three-dimensional multivariate model forecast error. Accordingly, the overall improvements to NWP models (like the RAP) represent the accumulated effect of many modifications. The individual RAP modifications described here were an outcome from individual hypotheses that were accepted or rejected based on case study testing and longer-period retrospective or parallel real-time testing, and the overall RAP improvements presented in this paper reflect integrated effects from these advances in the RAP since its inception in 2012.

2. GSI and DFI components for RAP data assimilation

The RAP uses the GSI, a data assimilation system (Wu et al. 2002; Whitaker et al. 2008; Kleist et al. 2009) with variational, ensemble, and hybrid ensemble-variational (used for RAP) options. The GSI is applied at NOAA/NCEP for both global (Global Forecast System; NCEP 2003) and regional (RAP, NAM, HRRR) applications. Use of the GSI for the RAP takes advantage of community GSI development and makes RAP-developed enhancements available for other NOAA models and the general research community.

The RAP application of GSI is unique in that it is within a 1-h assimilation cycle. The effectiveness of the RAP 1-h data assimilation cycle to produce sufficiently noise-free 1-h forecasts depends on the combination of sufficient multivariate balance from GSI and application of a digital-filter initialization [(DFI); application to RAP described by Peckham et al. (2016)]. The prognostic and analyzed variables in the RAP are listed in Table 3.

The background field of RAP data assimilation is the previous 1-h RAP forecast, as shown in Fig. 2, along with other components of the RAP assimilation cycle. Information from the larger-scale global GFS model is introduced every 12 h by a partial cycling technique to provide better longwave representation not available via regional data assimilation unable to use the full global set of observations. (Full regional cycling over the large RAP domain gave decidedly poorer results in an early experiment—results not shown.) In this partial cycling, a parallel RAP 1-h cycle is started at 0300 and

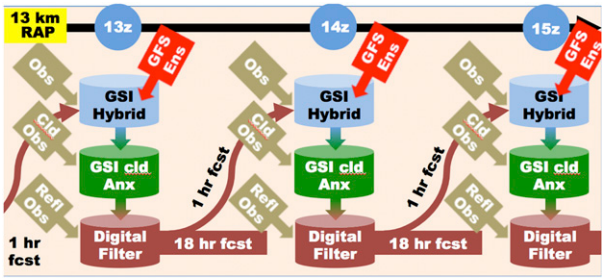

FIG. 2. Flow diagram for the Rapid Refresh. The maroon components are for the RAP model using WRF and DFI. Brown-like tilted boxes indicate observation types [reflectivity (refl), cloud (cld—nonprecipitating) and precipitating (from radar) hydrometeor observations, and all other observations, described in Table 4] for the three assimilation components. GSI data assimilation includes both hybrid EnKF-var assimilation (light blue) using the GFS 80-member ensemble (GFS Ens—red) to define the ensemble-based background error covariance and the cloud and hydrometeor (for both cloud and precipitation) component (green).

TABLE 4. Observational data used in the RAP version 3 as of September 2015. Symbols are as defined in Table 3, except RH is relative humidity with respect to water, V refers to horizontal wind components, T is temperature, p_s is surface pressure, and T_d is dewpoint.

Data type	Variables	~No.	Frequency
Rawinsonde (including special observations)	T, RH, V, z	125	12 h
NOAA 405-MHz profiler wind (decommissioned 2014)	V	~21 (2013)	1 h
Boundary layer (915 MHz) profiler wind	V, T_v	~30	1 h
Radar-VAD winds (WSR-88D radars)	V	125	1 h
Radar	Reflectivity, radial wind		1 h
Lightning	Flash rate converted to reflectivity		1 h
Aircraft	V, T	3000–25 000	1 h
Aircraft	q_v	0–1000	1 h
Surface/METAR—land	V, p_s, T, T_d	2200–2500	1 h
Surface/METAR—land	Ceiling/vis	2200–2500	1 h
Surface/mesonet—land	V, p_s, T, T_d	10 000–16 000	1 h
Buoy/ship	V, p_s	200–400	1 h
GOES atmospheric motion vectors	V, p	2000–4000	1 h
GOES cloud top	p, T	~10-km resolution	1 h
AMSU-A/HIRS-4/MHS/GOES	Radiances		
GPS precipitable water	PW	300	1 h

1500 UTC each day with 3-h GFS forecasts valid at those times introduced as the atmospheric background instead of the corresponding RAP cycle. After parallel hourly spinup assimilation cycles are run for 6 h ending, respectively, at 0900 and 2100 UTC, the 1-h forecasts from the parallel spinup RAP cycle are substituted for those from the primary cycle as the background field for RAP assimilation. Lateral boundary conditions are

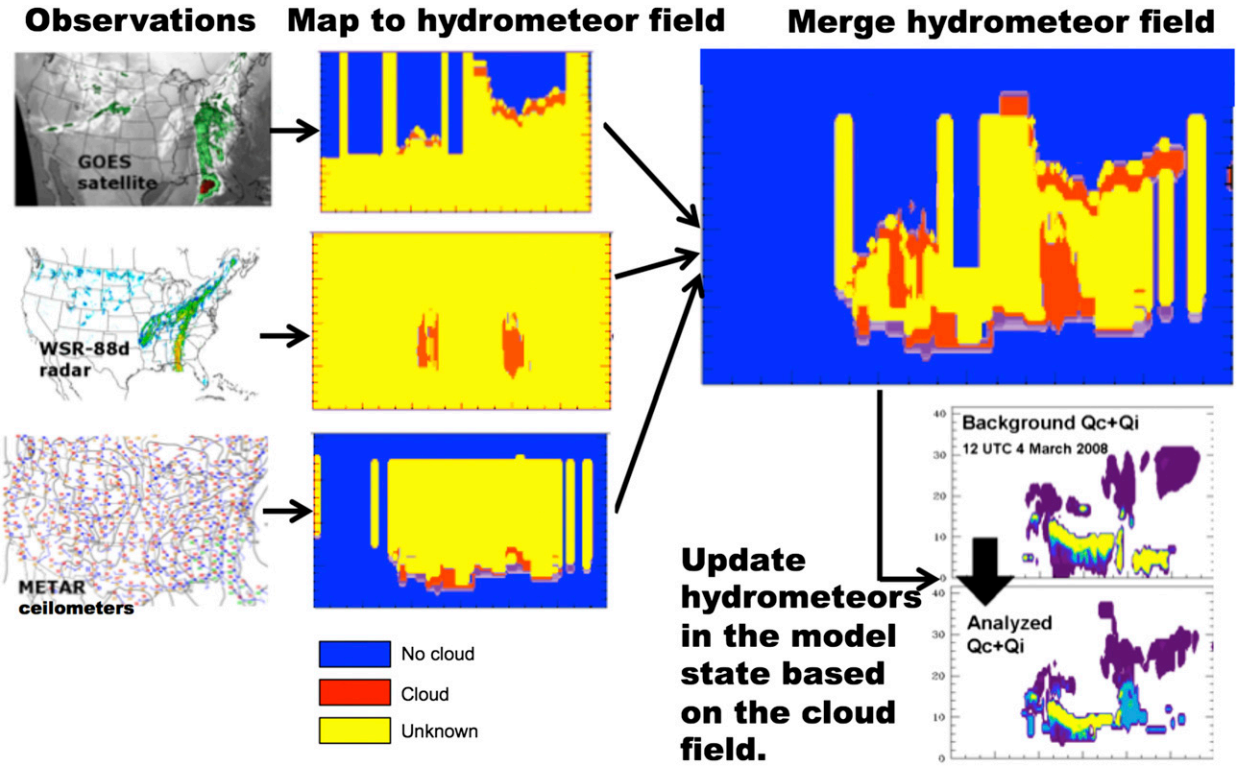

FIG. 3. Flowchart for 3D cloud and hydrometeor assimilation in the RAP as a GSI option. The blue–yellow–red plots are for a nominal vertical cross section with blue indicating cloud-free volumes, red indicating cloudy volumes, and yellow showing volumes with unknown cloud information. The respective yes–no–unknown volumes are shown for observations for (bottom) METAR cloud-ceiling and visibility observations, (middle) radar reflectivity, and (top) GOES cloud-top retrievals and brightness temperatures combined into a merged yes–no–unknown cloud and precipitation information field shown on the right. (bottom right) The colored areas show combined cloud water (Q_c) and ice (Q_i) mixing ratio before and after hydrometeor assimilation, nominal magnitude increasing from purple to blue to yellow.

TABLE 5. Variables updated in cloud and hydrometeor analysis for RAPv3.

Variables updated	Build cloud/hydrometeors in model 3D state?	Remove cloud/hydrometeors from model 3D state?	Which observations are used?
Cloud water, cloud ice, temperature, water vapor	Yes, below 1.2 km AGL	Yes	Satellite cloud-top pressure, ceilometers
Precipitating hydrometeors: rain water, snow, graupel	Yes: if 2-m $T < 5$°C, add to full column. Else, add at observed maximum reflectivity level and where observed reflectivity is between 15 and 28 dBZ	Yes	Radar reflectivity

specified from new GFS model runs initialized every 6 h. Data assimilation enhancements, most developed originally for the RUC (Benjamin et al. 2010) and related to DFI, radar, boundary layer, land surface, and cloud and hydrometeor fields, have been refined and included within GSI and used in the RAP, as described below.

a. Use of observational data and observation errors

The use of GSI for the RAP data assimilation system permits assimilation of additional observational data not previously incorporated into the RUC. In particular, full satellite radiance assimilation is now performed on an hourly basis in the RAP (over water and land and with bias correction to be described in a future paper). Observational data that are assimilated at hourly or longer intervals are summarized in Table 4. Observation errors are specified as in the NOAA NAM model. RAP observation time windows are narrow, appropriate for a 1-h cycle, generally from 45 min before analysis time to 15 min after analysis following the ~15-min offset. [Surface, rawinsonde, and aircraft data valid time are generally centered before the analysis time as described by Benjamin et al. (2004a), their section 3c.] A GSI forward-model option was developed and exercised for the RAP in which surface-temperature observations are adjusted based on the background lapse rate from the observation-station height to the model-terrain height. No adjustment is applied for 2-m dewpoint or 10-m wind observations; currently they are assimilated if surface pressure is no more than 15 hPa beneath the model surface pressure. A similar terrain-adjustment forward-model GSI option is applied to the GPS-retrieved total column water vapor to adjust its value to the model elevation at the GPS observation-station location, as used by Smith et al. (2007).

b. Background error covariance and hybrid options

The RAP version 1 (Table 2) used only a static background error covariance, combining balance from GFS-based background error covariance and variance together with horizontal and vertical impact scales from NAM background error covariance (Wu 2005) refined through RAP retrospective experiments. The RAP version 2 (Table 2) applies hybrid ensemble–variational assimilation (Wang 2010; Whitaker et al. 2008; Hamill and Snyder 2000) with half static background error covariance and half GFS data assimilation 80-member ensemble-based background error covariance. The ensemble component of the hybrid assimilation increases to 75% in RAP version 3. Even though the hourly RAP hybrid assimilation uses GFS EnKF ensemble forecasts available only four times per day, the use of hybrid assimilation significantly improves upper-air wind, moisture, and temperature forecasts (see section 6).

c. Application of digital-filter initialization in RAP

To reduce initial noise in 1-h forecasts and produce a more effective hourly assimilation, a backward–forward two-pass digital-filter initialization is applied within the ARW model (Peckham et al. 2016), similar to that applied to the RUC model (Benjamin et al. 2004a). A backward 20-min integration period is run first (inviscid, adiabatic), applying a digital-filter weighting over that period. Then, starting with that filtered field valid 10 min prior to analysis time, a forward 20-min integration with full physics is made, ending with another application of the digital filter to all prognostic fields. This filtering results in new fields valid at analysis time. The initial 3D hydrometeor fields and 3D water-vapor mixing ratio (using initial RH and DFI-output temperature) are then restored to maintain initial cloud fields where known (section 2e, below). This DFI application is shown to strongly reduce surface pressure oscillations from model mass-wind imbalance and improve accuracy of 1-h forecasts (Peckham et al. 2016), especially important for hourly cycling.

d. Radar reflectivity assimilation via latent heating

The RAP assimilates radar reflectivity on an hourly basis by a radar-DFI-latent-heating technique (Weygandt

TABLE 6. Model and physics configuration for RAPv3. Where applicable, ARW official release versions of physics routines are indicated.

Model and domain	
Model version	ARWv3.6+, nonhydrostatic = true
Domain	North America and surrounding area (Fig. 1)
Map projection	Rotated lat–lon
Grid points	954 × 835
Grid spacing	Nominal 13 km
Vertical computational layers	51
Pressure top	10 hPa
Lateral boundary conditions	Global Forecast System
Horizontal/vertical advection	Fifth-order upwind
Scalar advection	Positive definite
Large time step	60 s
Upper-level damping (for vertically propagating gravity waves)	Rayleigh (Klemp et al. 2008), dampcoef = 0.2 s^{-1}, zdamp = 5 000 m
Computational horizontal diffusion	Sixth order (0.12)
Run frequency	Hourly
Forecast duration	≥18h
Physics	
Radiation (longwave and shortwave)	RRTMG (v3.6) (Iacono et al. 2008)
Land surface	RUC LSM (v3.6+) (Smirnova et al. 2016)
Land use	MODIS 24 category
Planetary-boundary and surface layer	Mellor–Yamada–Nakanishi–Niino (v3.6+)
Boundary layer driven clouds (shallow Cu)	Grell–Freitas–Olson
Deep convection	Grell–Freitas (v3.6+) (Grell and Freitas 2014)
Microphysics	Thompson–Eidhammer "aerosol aware" (v3.6) (Thompson and Eidhammer 2014)
Microphysics tendency limit	0.01 K s^{-1}

and Benjamin 2007; Weygandt et al. 2008) applied previously to the hourly updated RUC model. This technique is central to the effectiveness of the RAP and the related 3-km HRRR model, especially for convective storms. Key is the 3D specification of latent heating, primarily from 3D radar reflectivity observations where available, applied within the 20-min forward DFI step with full physics (previous paragraph). Where latent heating can be estimated in 3D space with radar reflectivity data or proxy reflectivity data using a statistical relationship from lightning flash density (Benjamin et al. 2006), this estimate from observations is substituted for the prognostic temperature tendency of the precipitation-microphysics scheme used otherwise (including volumes of no radar echo) within this DFI forward step. Suppression of precipitation occurs by 1) forcing zero latent heating in no-echo volumes in the forward DFI step and by 2) deactivating parameterized convection in echo-free columns in the first 30 min of the free forecast. Otherwise, in volumes with no radar coverage, model latent heating is left unchanged. Latent heating is estimated by assuming a time period over which the radar-inferred condensate formed; values of 10–30 min have been tested in the RAP and RUC, and 10 min is currently used for this parameter (5 min was found to be too strong with excessive convection during the first 1–2 h). This radar-DFI assimilation is applied internally within the forecast model, after the rest of the RAP data assimilation. Radar- (and lightning) related latent heating is calculated within the GSI data-assimilation step and is constrained within the GSI by satellite cloud data for horizontal consistency.

e. Cloud and precipitation hydrometeor assimilation

METAR (cloud, ceiling, and visibility) observations and satellite-based retrievals of cloud-top pressure and temperature (currently GOES only) are used within the

TABLE 7. Sigma levels used with the ARW model in the Rapid Refresh (51 sigma levels, 50 computational levels).

1.0	0.9980	0.9940	0.9870	0.9750	0.9590	0.9390	0.9160	0.8920	0.8650
0.8350	0.8020	0.7660	0.7270	0.6850	0.6400	0.5920	0.5420	0.4970	0.4565
0.4205	0.3877	0.3582	0.3317	0.3078	0.2863	0.2670	0.2496	0.2329	0.2188
0.2047	0.1906	0.1765	0.1624	0.1483	0.1342	0.1201	0.1060	0.0919	0.0778
0.0657	0.0568	0.0486	0.0409	0.0337	0.0271	0.0209	0.0151	0.0097	0.0047
0.0000									

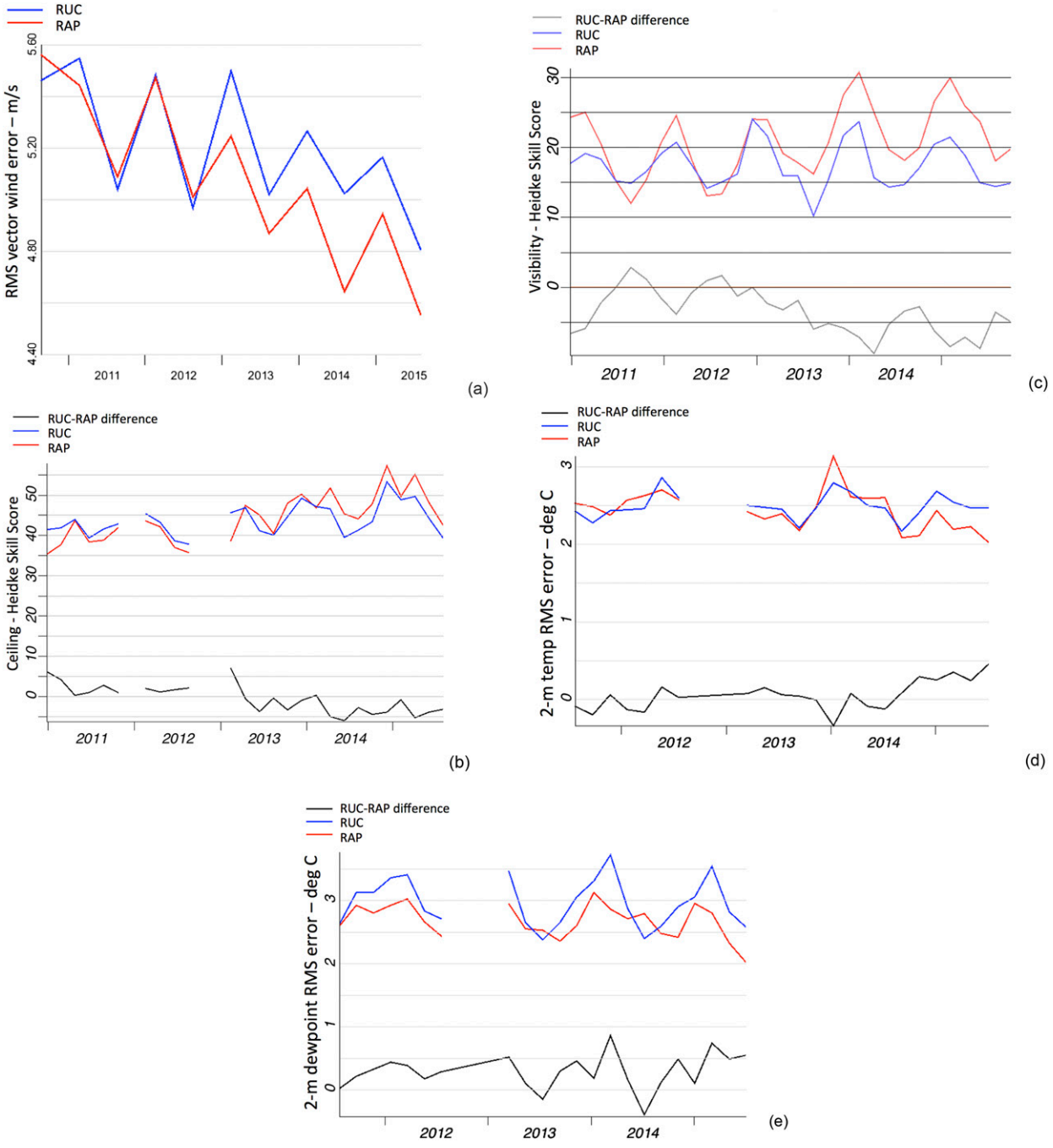

FIG. 4. Forecast error for RUC (blue, run at ESRL) and RAP-ESRL (red) model forecasts for 2010–15. RAP-ESRL change dates are identified in Table 1. (a) 250-hPa 6-h RMS vector magnitude wind forecast error. RAP-ESRL change dates are identified in Table 1. Verification is against rawinsonde observations over the RUC domain (CONUS) and is averaged over 6-month periods (October–March cold season and April–September warm season) and with all events matched. Periods with insufficient events for either model are left missing. (b) The 1000-ft ceiling Heidke skill score for 6-h forecasts. Verification is against METAR observations over the RUC domain (CONUS) and is averaged over 60-day periods and with all events matched. Periods with insufficient events for either model are left missing. Higher is more skillful. The difference (RUC − RAP) is also plotted in black. (c) As in (b), but for 1-mi visibility. (d) The 2-m temperature RMS 12-h forecast error (lower is better). Verification is against METARs over CONUS east of 100°W. Difference (RUC − RAP) is plotted in black. (e) As in (d), but for 2-m dewpoint.

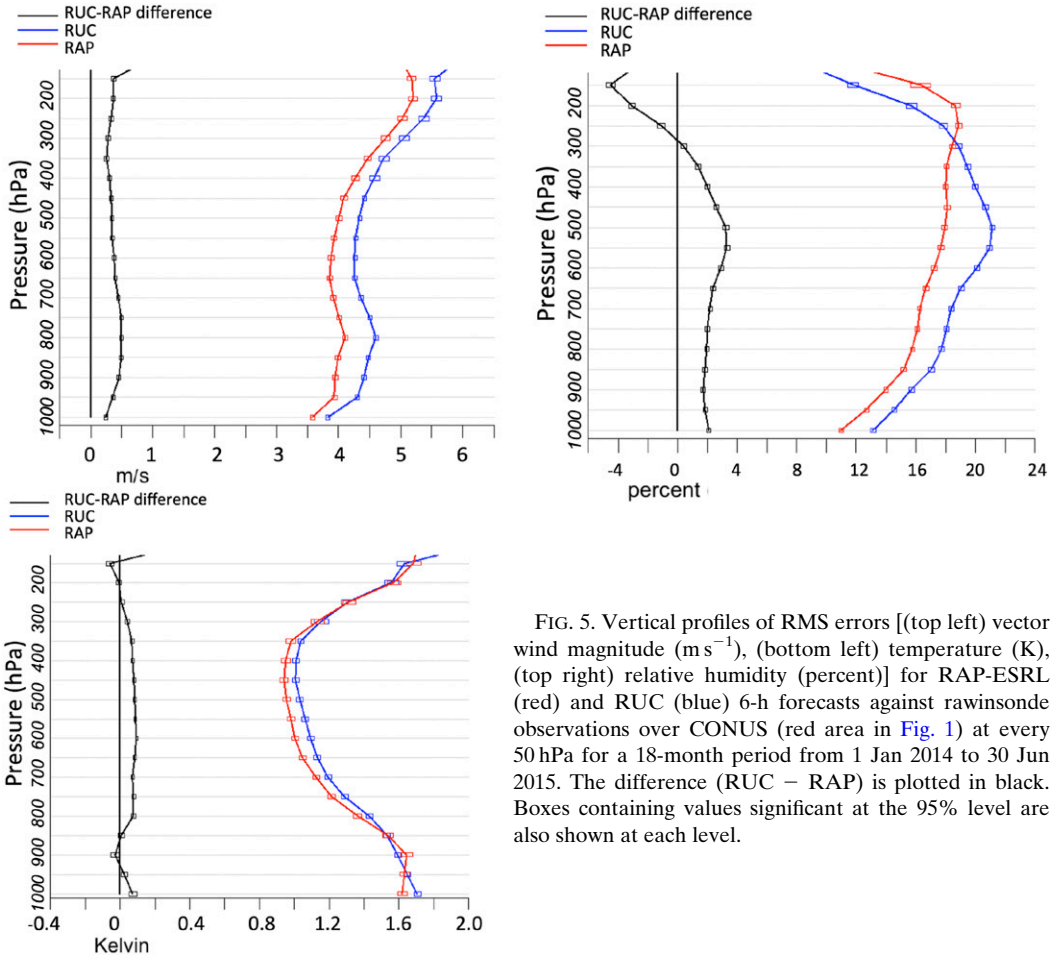

FIG. 5. Vertical profiles of RMS errors [(top left) vector wind magnitude ($m\,s^{-1}$), (bottom left) temperature (K), (top right) relative humidity (percent)] for RAP-ESRL (red) and RUC (blue) 6-h forecasts against rawinsonde observations over CONUS (red area in Fig. 1) at every 50 hPa for a 18-month period from 1 Jan 2014 to 30 Jun 2015. The difference (RUC − RAP) is plotted in black. Boxes containing values significant at the 95% level are also shown at each level.

RAP (via GSI) to modify background hydrometeor fields (Table 3) along with temperature and water-vapor mixing ratio to retain saturation or subsaturation as needed in volumes of cloud building or cloud clearing, respectively. This technique was initially applied to the RUC model/assimilation (Benjamin et al. 2004a) and is now applied to GSI assimilation for RAP. The schematic flow of the cloud–hydrometeor analysis is illustrated in Fig. 3. A three-dimensional cloud coverage observation information field (cloudy, clear, unknown) is generated each hour by using the METAR cloud base/coverage observations and satellite cloud top. Then, this cloud coverage is used to generate cloud ice and water based on environment conditions for areas of cloud building. This cloud water and ice information is then combined (Table 5) with 1-h forecast background 3D hydrometeor information to generate the final cloud water and ice 3D analysis fields. To ensure the cloud or clear information is retained in the forecast, the water vapor and temperature fields are adjusted (conserving virtual potential temperature) to match the cloud or clear condition at each 3D grid point where building or clearing is applied, respectively. Finally, 3D radar data are used to clear and build hydrometeors (up to 28 dBZ under conditions described in Table 5) starting with 3D rain, snow, and graupel precipitation hydrometeors from the 1-h background.

f. Near-surface assimilation including estimate of pseudo-innovations within the PBL

To enhance retention of surface dewpoint and temperature observations accounting for their likely vertical representativeness, an optional (via namelist) enhancement to GSI was developed in which surface innovations (observation–background differences) are extended upward toward the PBL (planetary boundary layer) top, creating pseudo-innovations. Initial innovations are created for surface 2-m temperature and dewpoint observations. In RAPv3, background values are estimated using flux-based diagnostic values of 2-m temperature and 2-m water-vapor mixing ratio from the WRF Model (instead of prior values at lowest model

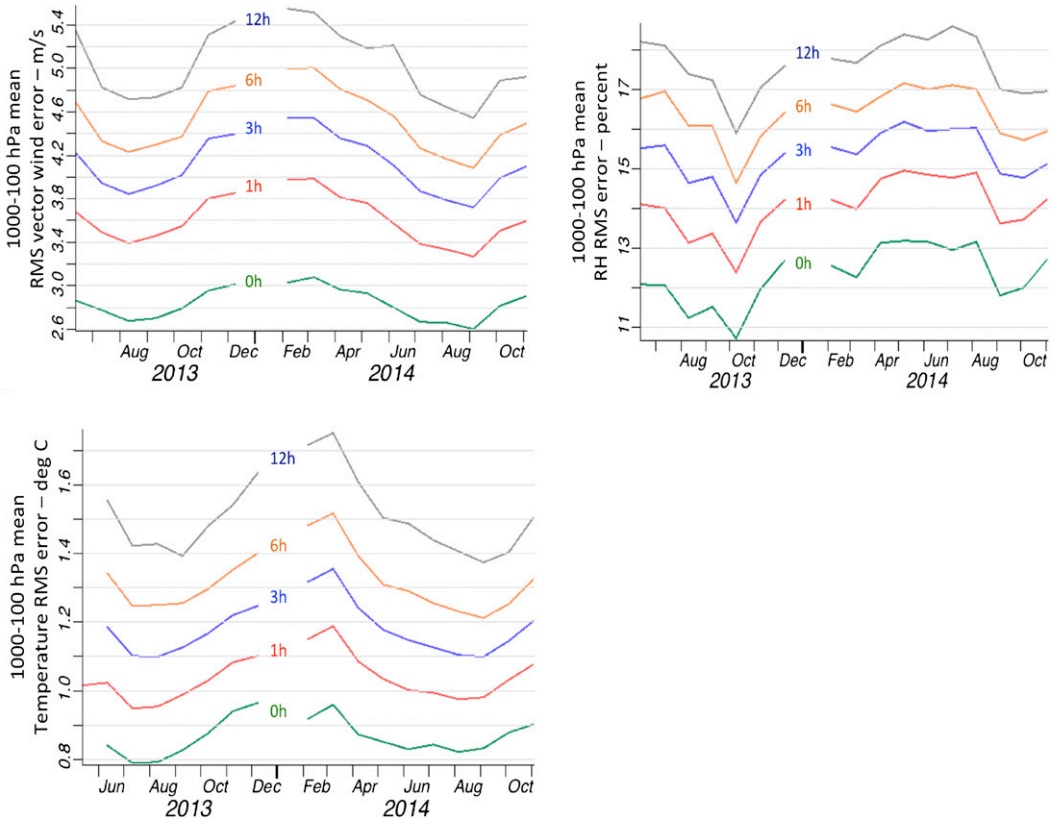

FIG. 6. Time series for RAP-ESRL forecast RMS errors [(top left) vector wind magnitude ($m\,s^{-1}$), (bottom left) temperature (K), and (top right) relative humidity (%)] as verified against hourly aircraft observations for durations of 0 h (analysis—green), 1 h (red), 3 h (blue), 6 h (orange), and 12 h (black). Error is averaged over 30-day periods over the 2-yr period from May 2013 through November 2014 and for all aircraft observations over CONUS from 1000 to 100 hPa. Only RH observations taken during descent are used for verification because they are more accurate than observations during ascent (W. Moninger 2015, personal communication). Isobaric output of RAP forecast fields are used here.

level at about 8 m above ground level). Pseudo-innovations are created every 20 hPa upward until reaching 75% of the PBL top (diagnosed from the previous 1-h RAP forecast) at the nearest grid point in the background forecast, as described by Benjamin et al. (2004d, 2010). Pseudo-innovations are created and assimilated for 2-m dewpoint starting with RAPv2 and those for 2-m temperature were added starting with RAPv3 (Table 8). This PBL-based pseudo-innovation technique is a simple and effective method for spreading information from surface observations vertically in well-mixed situations, to be replaced in future RAP versions by ensemble data assimilation with adaptive covariance in the PBL.

g. *Soil–snow temperature and soil moisture adjustment*

Similar to the use of pseudo-innovations within the planetary boundary layer to reflect vertical representativeness of surface observations, a simple coupled soil–air forecast-error relationship was created to estimate increments for soil and snow variables based on near-surface analysis atmospheric increments for temperature and moisture (Benjamin et al. 2004d; appendix A in this paper). Application of this covariance tends to retain the soil–air temperature difference from the forecast background field to the analyzed state. For soil–snow temperatures, near-surface analysis increments (driven largely by near-surface observations) are applied to the top five levels within the nine-level configuration in the RUC land surface model [LSM; Smirnova et al. (2016); section 3 below] soil domain and to the levels inside snow using the relationships described in appendix A. Soil temperature adjustment at the top level is limited to 1-K warming and to 3-K cooling. Parameters shown in appendix A were estimated through repeated parallel experiments with the RAP during both summer and winter periods.

Under the assumption that near-surface analysis increments for temperature and moisture of opposite sign

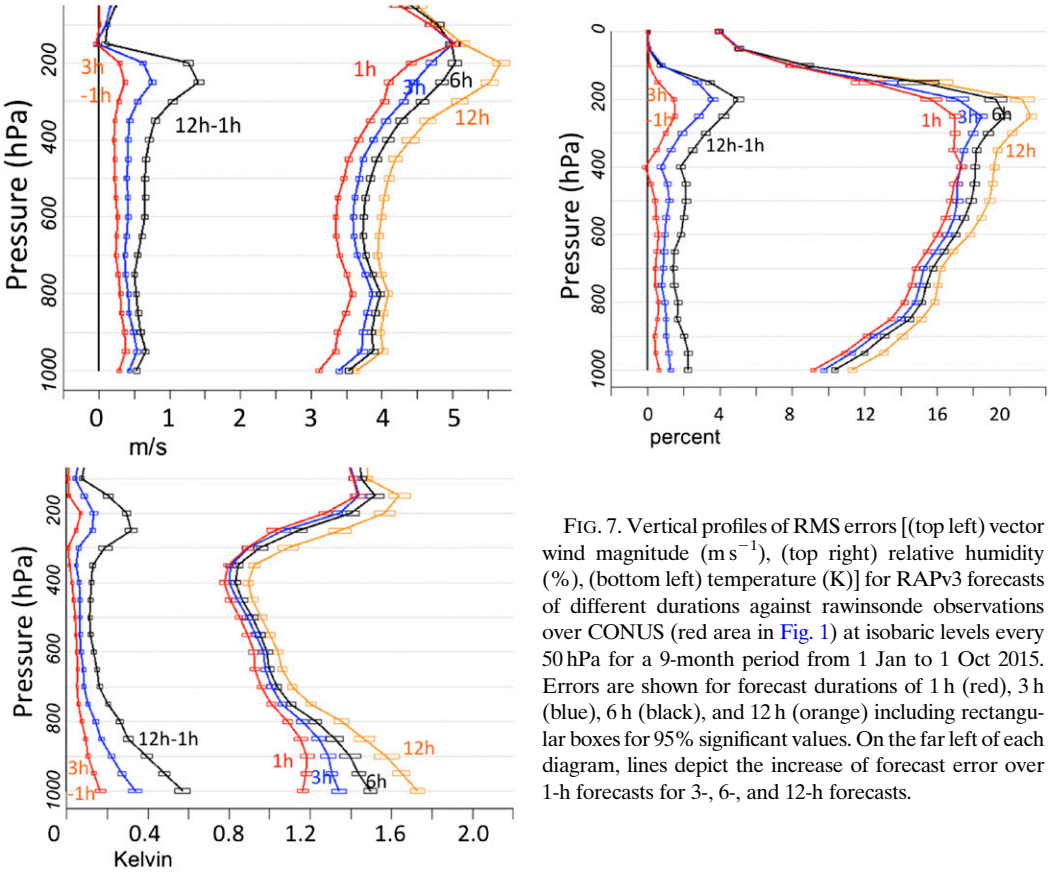

FIG. 7. Vertical profiles of RMS errors [(top left) vector wind magnitude ($m\,s^{-1}$), (top right) relative humidity (%), (bottom left) temperature (K)] for RAPv3 forecasts of different durations against rawinsonde observations over CONUS (red area in Fig. 1) at isobaric levels every 50 hPa for a 9-month period from 1 Jan to 1 Oct 2015. Errors are shown for forecast durations of 1 h (red), 3 h (blue), 6 h (black), and 12 h (orange) including rectangular boxes for 95% significant values. On the far left of each diagram, lines depict the increase of forecast error over 1-h forecasts for 3-, 6-, and 12-h forecasts.

(warm and dry, or alternatively, cold and moist) may be related to soil moisture errors under some conditions (daytime, no precipitation), a technique analogous to that for soil temperature was also developed to modify soil moisture (Benjamin et al. 2004d). This namelist-controlled option also added to GSI is applied only in daytime with no precipitation in the background forecast and with no snow on the ground. When the near-surface analysis increments both cool and moisten atmospheric conditions near the surface (meaning that the background forecast was too warm and dry), a small moistening is also applied to soil conditions in the top four levels of the land surface model. The opposite is also applied when near-surface analysis increments are to warm and decrease water-vapor mixing ratio. Equations for soil moisture analysis adjustment are also described in appendix A.

3. WRF Model component for RAP numerical weather prediction

The Rapid Refresh uses the Advanced Research version of WRF (ARW) dynamical core (Skamarock et al. 2008) as its model component on a 13-km grid over North America (Fig. 1). The ARW core offers rigorously tested numerical methods with capability for nonhydrostatic applications (a flexible, modularized code design, and refinement from the WRF user community, including a variety of physics options). Table 6 lists major attributes of the current configuration of the RAP model. This section describes the configuration choices and the rationale for their use in the RAP.

ARW for RAP was configured similarly to the RUC to provide accurate forecasts of clouds and boundary layer structure (important for aviation, severe-weather, and energy applications). Vertical layers were specified (Table 7) to give two benefits: 1) high vertical resolution very close to the surface to capture near-surface inversions and to avoid incorrect mixing out of surface-based shallow cold air during the forecast and 2) high vertical resolution near typical jet aircraft en route altitudes (approximately between 300 and 200 hPa). The hybrid sigma–isentropic coordinate in the RUC (Benjamin et al. 2004c) with adaptive vertical resolution provided this second beneficial feature, owing to the common presence of the tropopause in the 300–200-hPa

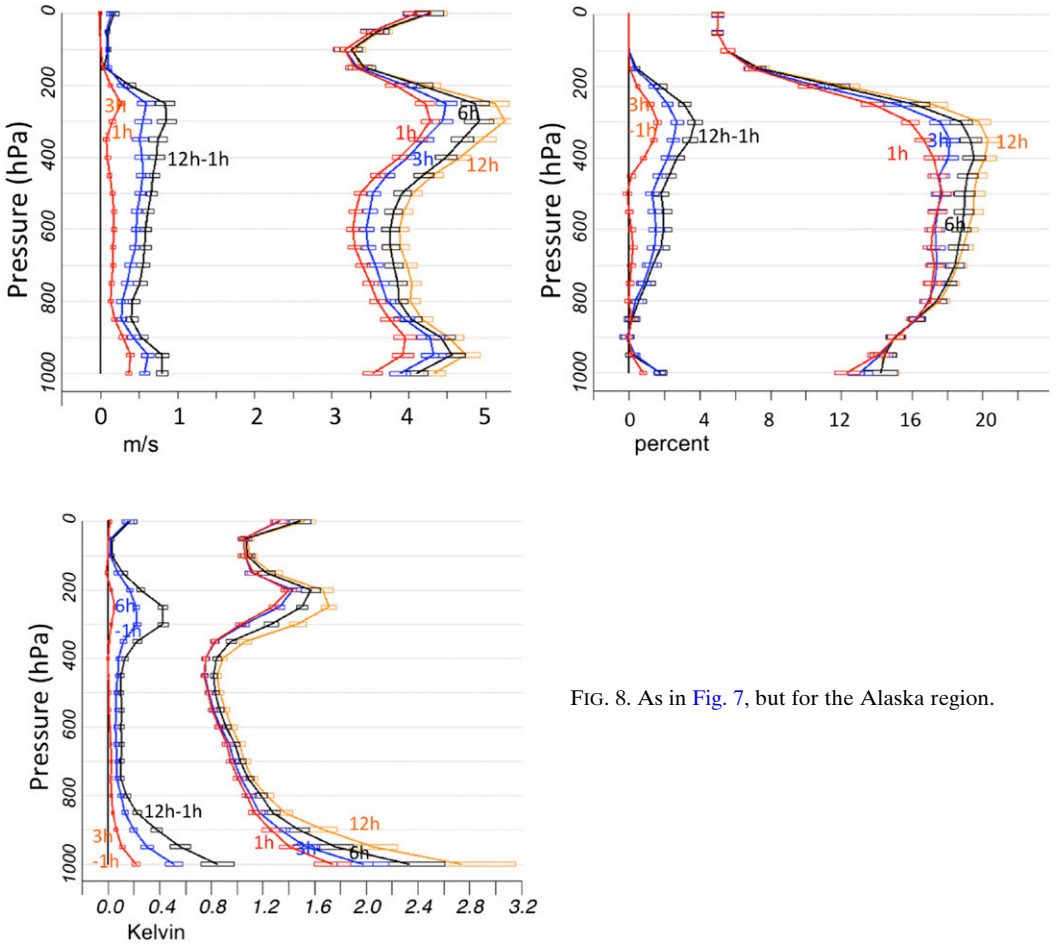

FIG. 8. As in Fig. 7, but for the Alaska region.

range. In contrast, the ARW uses a traditional sigma-*p* vertical coordinate (Phillips 1957), terrain following near the surface that smoothly becomes a constant pressure surface at the top of the model. In the case of the ARW, the sigma coordinate is expressed in terms of the hydrostatic pressure of the dry air mass.

Continuity in overall behavior of physical parameterizations was maintained in going from RUC to RAP with evolution as shown in Table 2. Because of the importance of in-flight icing as an aviation hazard, the RAP follows the RUC for cloud-precipitation parameterization in using the mixed-phase bulk cloud microphysics of Thompson et al. (2008) for RAPv1 and RAPv2 and the aerosol-aware microphysics of Thompson and Eidhammer (2014) for RAPv3. These schemes include explicit prediction of mixing ratios of cloud water and ice, rain, snow, and graupel and number concentration of ice and rain and (starting with 2014 version) cloud water. The RAP uses an improved version of the RUC LSM (named for the model in which it was originally used but now used widely in various WRF applications; Smirnova et al. 1997, 2000, 2016). The revised RUC LSM scheme (Smirnova et al. 2016) used in RAP includes nine levels, increased from six as used in RUC. It improves treatment of snow providing better diurnal variation of 2-m temperature in all seasons and more accurate 2-m temperatures over snow (Smirnova et al. 2016). RAPv1 and RAPv2 used a parameterization of deep convection based on Grell and Devenyi (2002) but with a 3D ("G3" scheme) extension to allow some awareness of resolution scale [see also tests of G3 in Grell and Freitas (2014)]. Like the RUC, the RAP continued to use Mellor–Yamada local mixing schemes for the PBL, adopting the Mellor–Yamada–Janjic (MYJ; Janjić 1994, 2002) for RAPv1.

For radiation, Dudhia shortwave and Rapid Radiative Transfer Model (RRTM; Iacono et al. 2008) longwave parameterizations were used in RAPv1 and RAPv2, changing (Table 2) in RAPv3 to the more sophisticated RRTM Global (RRTMG) radiation scheme for both long- and shortwave radiation, which includes radiative effects of (climatological) aerosols. In addition, the RAP has adapted the Mellor–Yamada–Nakanishi–Niino (MYNN) (Nakanishi and Niino 2004, 2009)

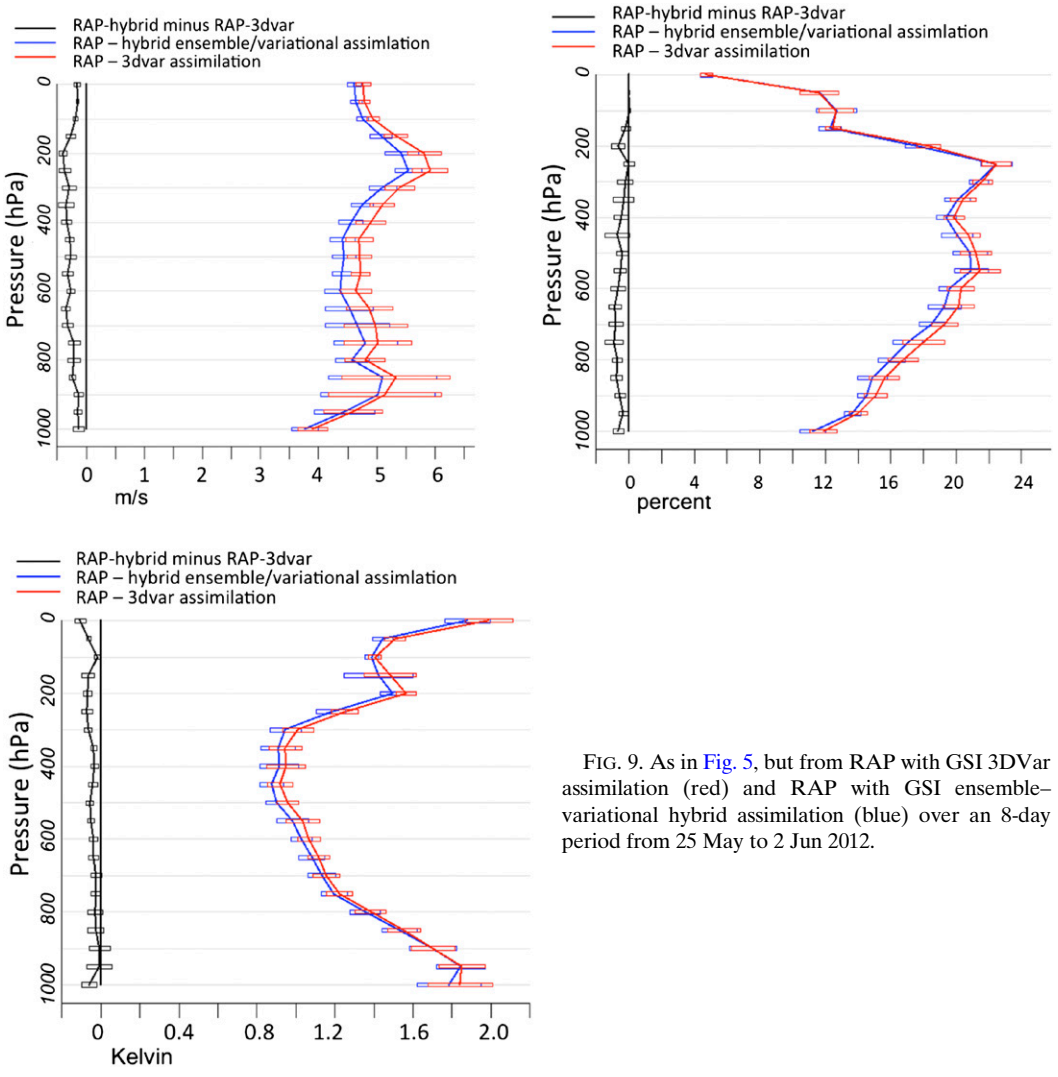

FIG. 9. As in Fig. 5, but from RAP with GSI 3DVar assimilation (red) and RAP with GSI ensemble–variational hybrid assimilation (blue) over an 8-day period from 25 May to 2 Jun 2012.

boundary and surface-layer schemes in RAPv2. Modifications to MYNN described in appendix B to remove numerical deficiencies and to improve the mixing-length formulation better account for relative importance of physical sources of turbulence under various conditions. These MYNN modifications address conditions ranging from very high stability typical of high latitudes in winter to deep warm-season dry-adiabatic mixed layers. A capability within the MYNN is enabled in RAP to represent subgrid-scale cloudiness that is often present at the top of boundary layers. This information is used for improved coupling to the RRTMG for attenuation of radiation.

With the aerosol-aware Thompson and Eidhammer (2014) precipitation microphysics used in RAPv3, the Cooper curve assumption (Cooper 1986; e.g., Thompson et al. 2008), relating the number of available ice nuclei to temperature given certain conditions on ice supersaturation, is replaced by an explicitly predicted supply of ice-friendly aerosol activated proportional to the amount of supersaturation and then removed by precipitation. An analogous prediction of water-friendly aerosol is used to predict the number concentration of cloud drops, which are then available to form rain through the collision–coalescence process. At present, the RAP is initialized with only a height and geographically dependent and seasonally varying climatological distribution of water- and ice-friendly aerosol available with this microphysics. This scheme opens the door for future RAP (and HRRR) developments to include weather-dependent sources and sinks of aerosols to produce a fully coupled aerosol–microphysics predictive system [e.g., WRF coupled with Chemistry (WRF-Chem); Grell et al. (2005)].

TABLE 8. Modifications made in RAPv3 to address warm–dry bias in RAPv2.

Model components	
MYNN boundary layer (section 3, appendix B)	Mixing-length parameter changed Numerical deficiencies removed Coupling boundary layer clouds to RRTMG radiation
Thompson cloud microphysics (section 3)	Changed to aerosol awareness for resolved cloud production (Thompson and Eidhammer 2014)
Grell–Freitas–Olson convective parameterization (section 3)	Shallow-cumulus radiation attenuation Improved retention of stratification atop mixed layer
RUC/Smirnova land surface model (section 3)	Reduced wilting point to allow more transpiration Keep soil moisture in cropland land-use areas above wilting point (effectively assuming background irrigation)
Data assimilation	
GSI modifications	Introduce use of temperature pseudo-innovations in boundary layer (section 2f) More consistent matching of surface observations and model background (2 m instead of 8 m; section 2f) Introduce cycling of canopy water from background to analysis field (Table 3)

In place of the G3 deep convection scheme used in RAPv1 and RAPv2, RAPv3 uses an updated version of the Grell and Freitas (2014) scale-aware deep convection scheme. This scheme is scale aware in the sense of relaxing the assumption traditionally used in mass-flux parameterizations of convection that updrafts and downdrafts occupy a negligible fraction of the cross-sectional area of a model grid column. For the 13-km RAP grid spacing, the scale-aware aspect has only a small impact, as scales resolvable by the numerical mesh are still far larger than the horizontal dimensions of a cumulonimbus updraft. The scheme is also capable of accounting for the role of aerosols on both the formation and evaporation of precipitation in updraft and downdraft through the impact of cloud-condensation nuclei on drop size distribution. This aerosol effect, in turn, impacts the partitioning of updraft condensate between conversion to precipitation and detrainment and subsequent evaporation to moisten the cloud environment.

Table 6 summarizes the RAP model configuration of ARW. Early testing of ARW for RAP used third-order vertical advection, but subsequent tests using fifth-order vertical advection demonstrated better maintenance of thin cloud layers (e.g., marine stratus) and slightly less smooth (i.e., more realistic) model-predicted sounding structures at very little added computational cost. In addition to activating the vertical-velocity damping option in the ARW, the magnitude of the potential temperature tendency coming out of the microphysics was constrained to be no larger than $0.01\,\mathrm{K\,s^{-1}}$. In the operational setting, this provides additional security against model crashes due to vertical Courant–Friedrich–Levy (CFL) violations resulting from moist convection. In addition, the sixth-order computational diffusion was activated, again with minimal impact on the well-resolved horizontal scales. The complete forecast configuration for the primary RAP cycle at ESRL can be found at http://rapidrefresh.noaa.gov/wrf.nl.txt.

4. Soil, snow, and water lower-boundary conditions

Specification of the RAP lower-boundary uses unique treatment and is strongly dependent upon ongoing cycling constrained by observations. The land surface nine-level model soil temperature and moisture fields have been cycled continuously in the RAP since 2010 (as was done in the RUC; Benjamin et al. 2004a). The atmospheric assimilation of radar reflectivity data to provide fairly accurate 1-h precipitation provides a strong constraint on evolution of the land surface fields in the RAP. Another strong constraint is the assimilation of cloud and hydrometeor fields (especially satellite-based cloud information) to define cloud cover. Hourly assimilation of other fields,

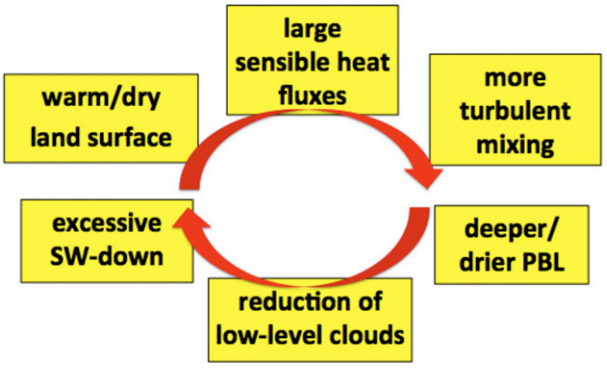

FIG. 10. Conceptual model of positive feedback model bias associated with RAPv2 warm and dry bias.

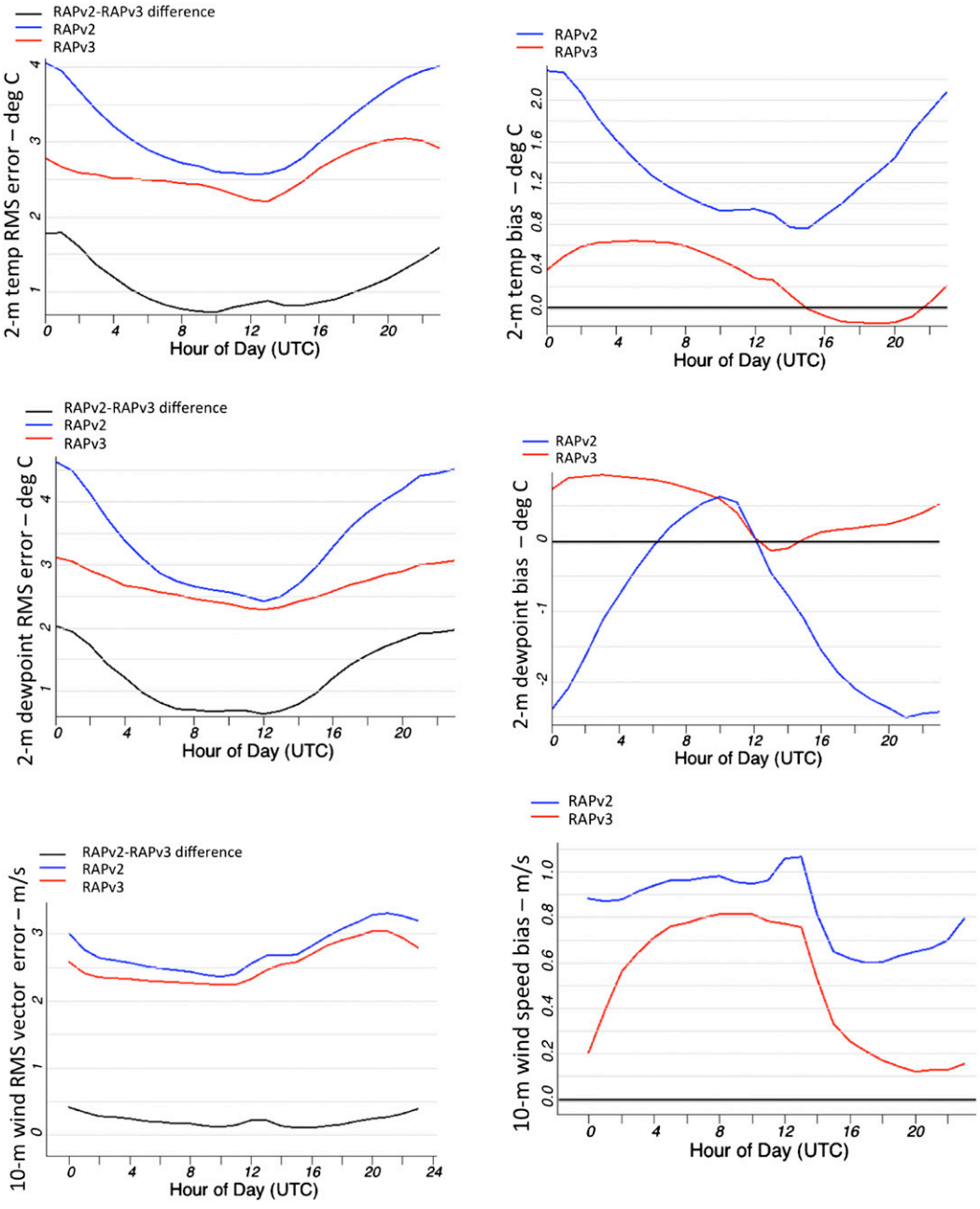

FIG. 11. Surface verification over the 4-month period from 1 May to 31 Aug 2015 for 12-h forecasts from RAPv2 and RAPv3 in eastern CONUS region for (left) RMS error and (right) bias over period. Both RMS errors and bias are calculated for forecasts vs METAR observations. Statistics in each column are for (top) 2-m temperature, (middle) 2-m dewpoint, and (bottom) 10-m wind magnitude.

especially near-surface observations (METARs and, to a lesser extent, mesonet; Table 4), also provides some constraint on the evolving land surface fields. In addition, the soil–atmosphere coupled data assimilation described in section 2g provides a significant constraint, correcting errors especially when applied repeatedly in the hourly update cycle.

Snow fields (snow water equivalent and snow temperature in the two-snow-layer component of the RUC LSM) in the RAP are also provided through ongoing cycling. Observation-based snow-cover modification is applied daily (usually 2300 UTC) through horizontal snow-cover trimming and building using the satellite-based daily updated NESDIS

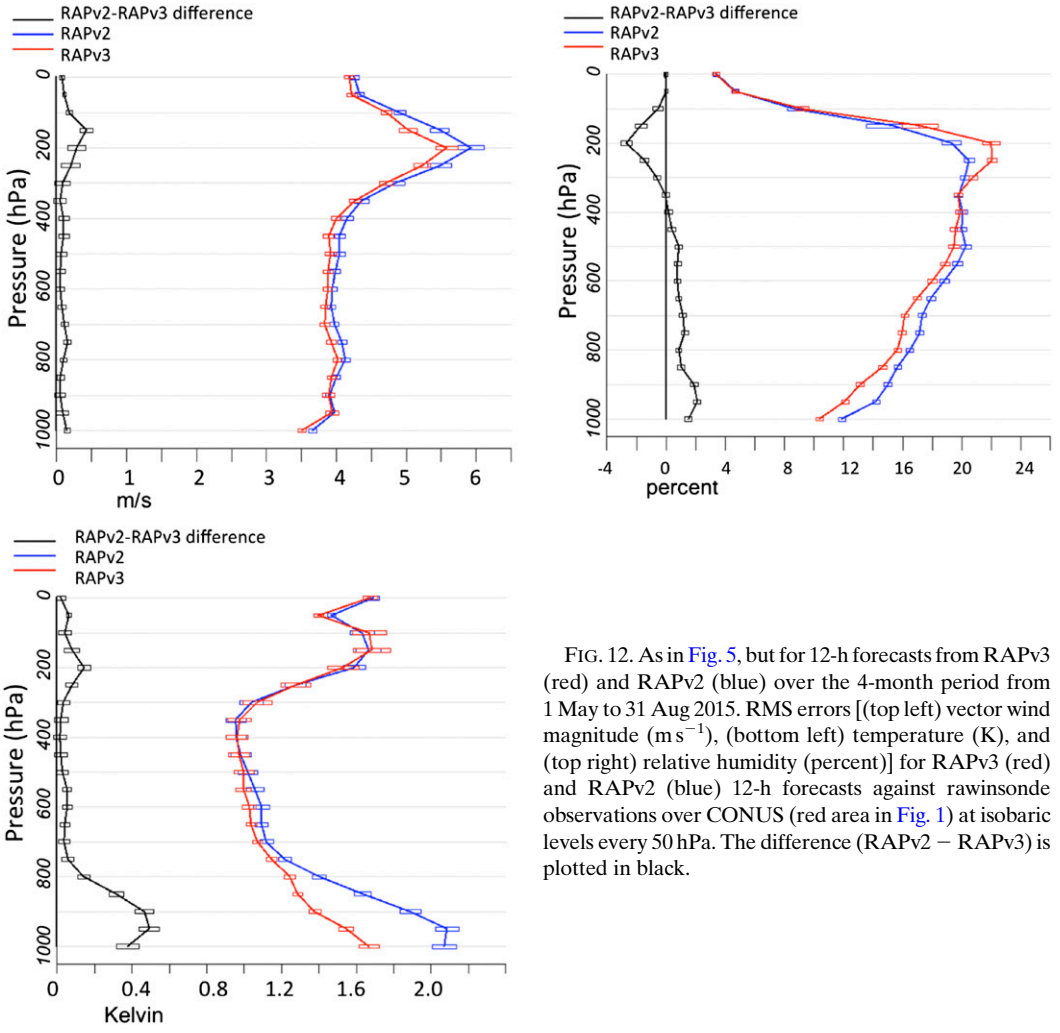

FIG. 12. As in Fig. 5, but for 12-h forecasts from RAPv3 (red) and RAPv2 (blue) over the 4-month period from 1 May to 31 Aug 2015. RMS errors [(top left) vector wind magnitude ($m\,s^{-1}$), (bottom left) temperature (K), and (top right) relative humidity (percent)] for RAPv3 (red) and RAPv2 (blue) 12-h forecasts against rawinsonde observations over CONUS (red area in Fig. 1) at isobaric levels every 50 hPa. The difference (RAPv2 − RAPv3) is plotted in black.

snow–sea ice data. These data are used to trim excessive snow cover on the ground via direct insertion (only if the forecast from the previous hour does not indicate snowfall at that grid point) and to build snow cover where needed to compensate for missed snowfall (Smirnova et al. 2016). This NESDIS product is also used to update RAP sea/lake ice coverage daily. No ice fraction data within grid cells were available at NCEP as of 2015.

Sea surface temperatures (SSTs) are specified from the NCEP global high-resolution SST analysis (http://polar.ncep.noaa.gov/sst/rtg_high_res). As of 2015, water surface temperatures for inland lakes other than the Great Lakes were found to be estimated more accurately from the NCEP North American SST (NAM_SST). A summary of sea–lake temperature specification in the RAP is provided at http://ruc.noaa.gov/rr/RAP_SST-snow.html.

5. Verification: RAP versus RUC

Ongoing multiyear comparisons between the RUC and RAP were conducted, even after the discontinuation of the NCEP RUC in May 2012. Examination of forecasts from the two models provides historical perspective on the evolution of RAP and RUC skill over time (Fig. 4). Changes to the RUC model ceased in 2011, except for changes in available observational data (substantial increase in aircraft data). A multiyear comparison of 6-h forecasts of 250-hPa wind over the CONUS between RAP and RUC is shown in Fig. 4a. Skill of RAP and RUC wind forecasts were similar from 2009–12 but better for RAP (smaller error) by 2013/14, indicating RAP improvement over the RUC baseline.

Jet-level wind accuracy is critical for RAP–RUC applications involving air-traffic management and flight planning (3–8-h duration forecasts used especially for

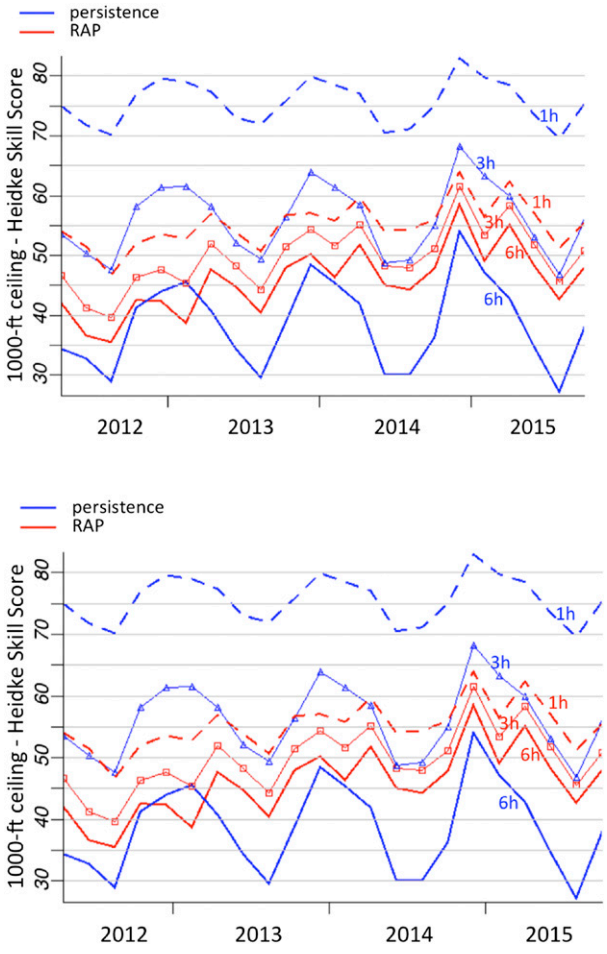

FIG. 13. Ceiling (top) 1000- and (bottom) 3000-ft Heidke skill score for RAP-ESRL model (red) and persistence (blue) forecasts for April 2012 through November 2015, verified against METAR observations over the CONUS. Verification is shown for forecast durations of 1, 3, and 6 h with dashed lines, thin lines with markers, and thick lines, respectively.

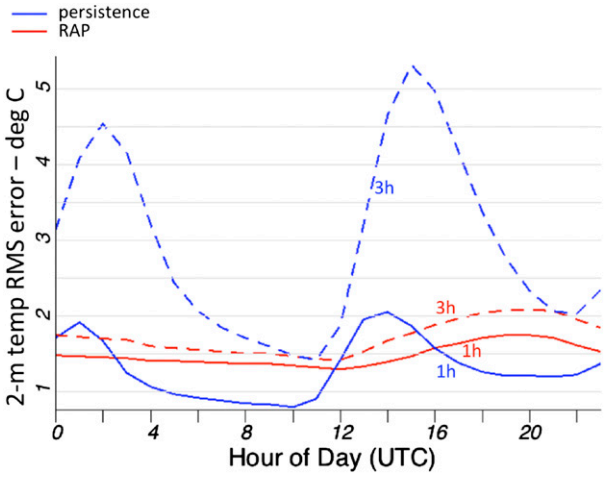

FIG. 14. The 2-m temperature forecast RMS errors for RAPv3 (red) and persistence (blue) 1-h (solid lines) and 3-h (dashed lines) forecasts for a 4-month period from June to September 2015. Verification is against METAR observations in the eastern United States (east of 100°W).

domestic routes). RMS wind vector forecast errors shown are larger in the cold (6-month October–March averaging in Fig. 4a) than the warm season (6-month April–September averaging). This seasonal variation is typical and related to stronger jet-level winds over the CONUS during the colder season. The downward trend in 6-h wind forecast error in the last few years for both models may be attributable to a large increase in aircraft data over the United States (WMO 2015); aircraft data have been the most significant observation type responsible for short-range hourly updated forecast skill (Benjamin et al. 2010).

Forecasts of another key aviation parameter—ceiling height for instrument flight rules (IFR) or 1000 ft (1 ft = 0.3048 m), evaluated by Heidke skill score—also show improved RAP skill over RUC for 2013/14 (Fig. 4b; negative RUC–RAP skill in black line at bottom indicates higher skill for RAP in that period). The most important modification for the RAP in 2013 was introducing the hybrid ensemble–variational data assimilation (in ESRL primary RAP configuration). The hybrid assimilation, included in RAPv2 at NCEP in Feb 2014 (Table 1; also see section 2b), was significant for improved upper-level winds (Fig. 4a, section 6, and Fig. 9) and possibly contributed to improved ceiling forecasts. Improved visibility forecasts are also evident in RAP versus RUC starting in 2013 (Fig. 4c), similar to that shown for ceiling. For surface forecasts, 2-m temperature 12-h forecasts started showing a clear improvement over RUC in late 2014 (Fig. 4d). For 2-m dewpoint forecasts, RAP has shown superior forecast skill (Fig. 4e) since 2011 with the exception of summer 2014.

A comparison between RAP and RUC 6-h forecast skill (errors versus rawinsondes) on isobaric levels was also made for upper-air forecasts of wind, relative humidity (RH), and temperature, covering an 18-month period from January 2014 to June 2015 (Fig. 5). For 6-h wind forecasts, RAP had lower RMS vector errors than RUC at all levels, with the difference ranging from 0.3 up to 0.5 m s^{-1}. For temperature, the RAP had smaller forecast error by about 0.1 K from 800 to 400 hPa and at 1000 hPa and similar skill to the RUC otherwise near the tropopause and in the 950–850-hPa layer. For RH, the RAP had smaller forecast error by 2%–3% from the surface up to 400 hPa. The RAP had larger RH error than RUC for 200–100-hPa levels, where

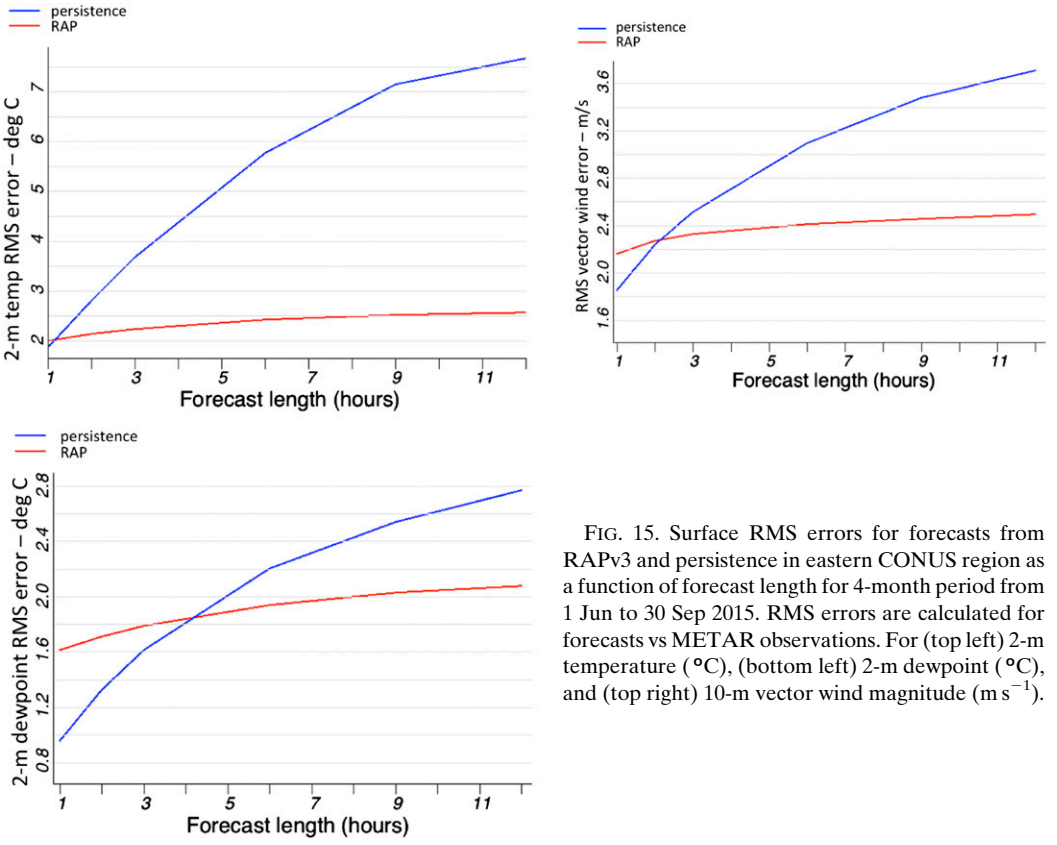

FIG. 15. Surface RMS errors for forecasts from RAPv3 and persistence in eastern CONUS region as a function of forecast length for 4-month period from 1 Jun to 30 Sep 2015. RMS errors are calculated for forecasts vs METAR observations. For (top left) 2-m temperature (°C), (bottom left) 2-m dewpoint (°C), and (top right) 10-m vector wind magnitude ($m\,s^{-1}$).

rawinsonde observational accuracy is lower and where clouds are infrequent. The RUC may have had an advantage in this near-tropopause layer due to its isentropic vertical coordinate.

6. Verification: Effects of recent assimilation and model changes and degradation of skill for longer forecasts

Hourly aircraft observations are available over the United States, providing an opportunity for verification to measure hourly updated RAP forecast skill. The same forecast duration comparisons can be calculated against rawinsonde observations (Benjamin et al. 2004a), but those include valid times only at 0000 and 1200 UTC. Aircraft observations, despite having diurnal variations in volume and irregularity in spatial distribution, can provide a broader round-the-clock look at RAP forecast skill than rawinsondes, verifying forecasts 24 times daily compared to twice daily (0000–1200 UTC) for rawinsondes. The results provided in Fig. 6 show a 2013/14 RAP forecast skill comparison differentiated by forecast duration, using aircraft observations and 30-day averaging. The figure shows that a monotonic decrease of forecast error occurs as forecast length decreases from 12- through 1-h forecasts. This result is central to justifying a 1-h NWP cycle to improve situational-awareness forecasting. Lack of balance without initialization (like DFI used for RAP; section 2), aliasing from irregular observation distribution (especially for aircraft data), and inadequate data assimilation design can all cause noisier 1-h forecasts with poorer forecast skill (Peckham et al. 2016).

This error decrease with decreasing forecast length all the way down to 1-h forecasts occurs similarly for wind, temperature, and relative-humidity forecasts and for all seasons. The effect of hourly assimilation (per 12–1-h forecast-error difference) is stronger in cold seasons. In addition, there is a seasonal variation

TABLE A1. Coefficients for soil temperature adjustment from atmospheric increment (A1) as a function of level in the land surface model.

k	$\alpha(k)$ for nine-level configuration	$\alpha(k)$ for six-level configuration
1	0.60	0.60
2	0.55	0.40
3	0.40	0.20
4	0.30	
5	0.20	

TABLE A2. As in Table A1, but for soil moisture adjustment [in (A3)].

k	$\alpha(k)$ for nine-level configuration	$\alpha(k)$ for six-level configuration
1	0.2	0.2
2	0.2	0.2
3	0.2	
4	0.1	

of forecast error, with higher error in the cold season for wind and temperature, and in general, higher error for the warm season for RH. An explanation is that for CONUS, stronger gradients and short-range changes of wind and temperature in the cold season are related to more frequent passages of stronger frontal dynamic systems. For RH, larger forecast error in the summer is expected from greater contribution from small-scale convective activity in the warm season compared to the contribution from frontal dynamics. The analysis fit to observations, also shown, exhibits a similar annual cycle.

Examination of the variation in forecast skill (as verified against rawinsonde observations) by vertical levels (Fig. 7) reveals that the monotonic improvement in forecast skill with decreasing forecast duration (due to the assimilation of more recent observations and use of more recent boundary conditions) is manifest at all vertical levels. Forecast-error reduction with decreased lead time is greatest at upper levels for wind (i.e., jet stream altitudes, where errors are largest) and in the lower troposphere for temperature and relative humidity. Likewise, even over Alaska, with its observational sparseness compared to the CONUS, the RAP produces more accurate forecasts at a progressively shorter forecast duration for temperature, RH, and winds (Fig. 8). Overall, the results in this section demonstrate that, despite irregular hourly observation distribution, more accurate forecasts are produced by RAP at shorter duration from a variety of perspectives: across regions (CONUS vs Alaska), in different times of year, across different vertical levels, and for different variables (i.e., wind, temperature, and RH).

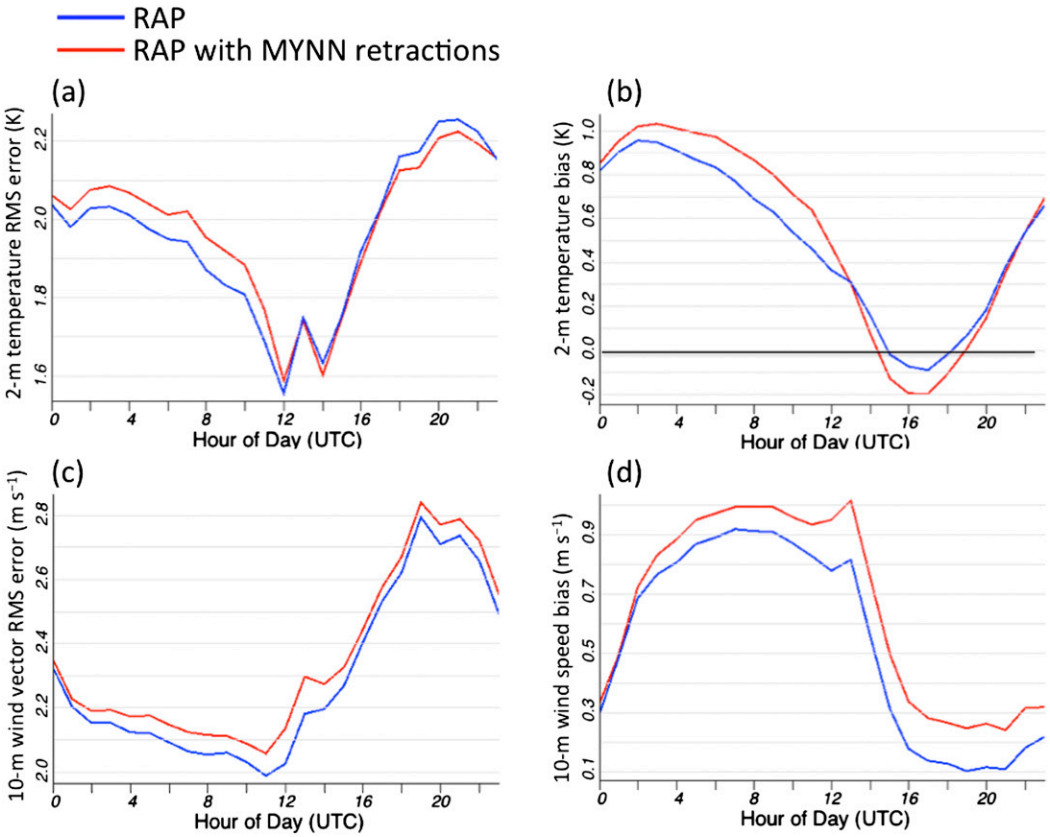

FIG. B1. Surface verification as in Fig. 11, but for a 16–22 Jul 2014 test period and for RAPv3 control (blue) and a RAPv3 experiment (red) with MYNN scheme enhancements withheld (described in appendix B). RMS error is shown in left column for (a) 2-m temperature and (c) 10-m wind (RMS vector magnitude). (right) Bias error is shown for (b) 2-m temperature and (d) 10-m wind speed.

Introduction of the hybrid ensemble–variational assimilation (see section 2b) into the RAP replacing the previous 3DVar provided a significant improvement in 6-h forecast skill at all levels and for wind, RH, and temperature according to results from a 9-day controlled experiment (Fig. 9). The differences in skill (black lines in Fig. 9) are significant to the 95% level. Further experiments on RAP data assimilation with the hybrid technique will be described in a future paper.

Modifications in RAPv3 (Table 2) in model physics and data assimilation (summarized in Table 8) were largely designed to reduce certain systematic forecast biases, including a daytime, low-level warm and dry bias over the central and eastern CONUS during the warm season. The processes contributing to this bias are summarized in Fig. 10, where insufficient model-state cloud coverage results in excessive downward solar radiation and warm–dry conditions near the surface (and accumulated in the land surface). The subsequent excessive growth of the PBL, and the entrainment of dry free-atmosphere air into the PBL, can further decrease PBL-top cloudiness. The key objective of these modifications was to increase overall shortwave attenuation from 1) improved representation of subgrid-scale clouds (MYNN scheme—appendix B, and shallow cumulus in the Grell–Freitas scheme), 2) more accurate grid-scale clouds [via introduction of the Thompson and Eidhammer (2014) aerosol-aware microphysics scheme], and 3) the representation of clear-sky aerosols. Use of the improved surface assimilation in RAPv3 as described in section 2f also contributes to this improvement.

A significant reduction in 12-h forecast error for 2-m temperature and dewpoint (Fig. 11) resulted from these RAPv3 changes, especially during daytime. Both RMS and bias errors are reduced (1–2 K during daytime, 0.5–1.0 K during night) in RAPv3. Ten-meter wind speed bias errors are also reduced significantly, especially during daytime. These error reductions in RAPv3 are vertically robust (Fig. 12), with lower-tropospheric reductions in RH RMS error of 1%–2% and in temperature RMS error of 0.4–0.5 K. Almost all of these improvements are statistically significant at the 95% level. Overall, the model and assimilation changes in RAPv3 as shown in Table 8 have proven effective at producing more accurate forecasts, especially near the surface and within the lower troposphere.

7. Verification against persistence forecasts

Persistence forecasts are difficult to improve upon for very short forecast durations and provide formidable competition for forecasts of only a few hours (e.g., Jacobs and Maat 2005). Persistence and extrapolation forecasts have better skill over an NWP forecast at the shortest time durations (Anthes and Baumhefner 1984; Mittermaier 2008). However, the crossover time, the time at which NWP skill exceeds persistence and extrapolation, has decreased with vastly improved data assimilation and model accuracy. In this section, the RAP forecasts of varying durations are compared against persistence forecasts at METAR stations in order to determine the skill crossover time.

RAP ceiling forecasts are compared against persistence for 1000-ft (IFR) and 3000-ft [marginal visual flight rules (MVFR)] events (Fig. 13) using METAR observations for verification as well as station-specific persistence forecasts. For 1000-ft ceiling forecasts (Fig. 13a), persistence forecasts clearly have greater skill than RAP forecasts at 1-h duration and slightly more skill at 3-h duration in cold season during this comparison time window. Skill is about equal at 3 h in the warm season for 2014 and 2015. This result suggests that the crossover time at which RAP exceeds persistence skill is approximately 3 h for the 1000-ft ceiling forecast in the warm season and about 3.5–4 h for the cold season. At 6-h forecast duration, the RAP model demonstrates decidedly more skill than persistence in forecasting 1000- and 3000-ft ceilings. Results are similar for 3000-ft ceiling forecasts with nearly equal skill between 3-h RAP and persistence forecasts in 2015 and with slightly better persistence skill in winter. Overall, for both 1000- and 3000-ft ceiling forecasts, the crossover time is about 3 h in summer and 4 h in winter. Preliminary testing of station-based postprocessing to HRRR ceiling and visibility forecasts using LAMP (Ghirardelli and Glahn 2010) show effective results in winter (Ghirardelli et al. 2015) and summer (Glahn et al. 2015).

A comparison of RMS error for RAP 2-m temperature forecasts and persistence forecasts by time of day is presented in Fig. 14. Persistence forecasts are again specified by station (METAR) observed values and not analysis values. For this variable, 1-h persistence forecasts have slightly lower RMS error than 1-h RAP forecasts midday and at night but worse at diurnal temperature transition times. For 3-h forecasts, RAP NWP forecasts are more accurate than persistence forecasts. Overall, the skill crossover time for 2-m temperature ranges from 0.5 h at diurnal change times (morning and early evening) to about 2 h midday and midnighttime.

Finally, the forecast RMS errors as a function of lead time are examined for persistence versus RAP forecasts for 2-m temperature, 2-m dewpoint, and 10-m wind (Fig. 15). The skill crossover time averaged over 24-h periods is about 1 h for 2-m temperature, about 4 h for dewpoint temperature, and about 2 h for 10-m wind.

8. Future of RAP

The Rapid Refresh hourly updated assimilation and modeling system provides substantial improvement over the previous hourly updated model at NOAA, the Rapid Update Cycle model. The RAP is an anchor for tactical forecasting in the United States, including decision-making related to severe weather, aviation, and renewable energy (Wilczak et al. 2015). The hourly RAP is used as situational-awareness information for many NOAA aviation hazard products (http://aviationweather.gov/adds) and the NOAA Storm Prediction Center Mesoscale Analysis (http://www.spc.noaa.gov/exper/mesoanalysis/). The RAP is the parent model for its 3-km counterpart model: the High-Resolution Rapid Refresh (HRRR) model. For now, the RAP provides most of the initial condition information used by the HRRR model, but future versions of the HRRR will include more cycling at its 3-km grid resolution. The time scale or lifetime of many weather phenomena can be under 3 h down to several minutes or less (e.g., individual clouds, eddies, etc.)—a motivation for rapid updating NWP using recent observations to represent the current situation in the model state for these phenomena.

Experiments are currently underway with regional ensemble data assimilation to examine the efficacy of improved covariances with cloud and hydrometeor-related variables compared to the current global-model-provided ensemble data for background error covariance. It is likely that hydrostatic-scale regional models, including the RAP, will be phased out in upcoming years owing to the increased skill of nonhydrostatic models and computational advances. Nevertheless, the RAP has clearly established a benchmark for the best possible hourly updated NWP forecast skill within its domain. The crossover time for skill between a model forecast system versus persistence is now generally between 1 and 4 h. Data assimilation and modeling techniques described here have enabled that level of performance. The RAP has set a new standard for short-range forecast performance to guide decision-making for many safety and economic activities. The HRRR model (Smith et al. 2008), now a convection-permitting, hourly updated model at NCEP in its own right, will be described in a closely related article in the near future.

Acknowledgments. The RAP was developed under significant support from NOAA, the Federal Aviation Administration (FAA), and the Department of Energy. We thank Isidora Jankov, Hongli Jiang, and John Osborn of NOAA/ESRL for helpful reviews. We also thank three anonymous reviewers and the journal editor for extremely thorough and very thoughtful reviews of the manuscript.

APPENDIX A

Soil Adjustment within Atmospheric Data Assimilation

These relationships are applied in GSI to modify multilevel soil temperature and moisture after the atmospheric analysis increment is calculated, also described above in section 2g.

1) The soil–snow temperature adjustment is calculated as

$$\Delta T_s(k) = \alpha(k)\Delta T_a, \tag{A1}$$

where ΔT_a is the atmosphere temperature analysis increment in K at the lowest model level. The $\Delta T_s(k)$ is the soil–snow temperature-adjustment value in K at the kth soil–snow level. The $\alpha(k)$ is the adjustment ratio for kth soil–snow level, and its values for current RAP–HRRR applications are listed in Table A1.

Soil temperatures are adjusted down to the level closest to 50 cm. For the nine-level soil model configuration (Smirnova et al. 2016), the top five levels are adjusted (down to 60 cm) while for six-level soil model configuration, the top three levels are adjusted (down to 40 cm). The snow temperatures at up to two levels (Smirnova et al. 2016) are adjusted with the same weighting as for the top soil level.

A maximum value for the soil temperature adjustment is set as 1 K, and the minimum value for the soil temperature adjustment without snow is set by

$$\mathrm{Min}\Delta T_s(k) = -2.0 \times \left(1.0 + \frac{T - 283.0}{15.0}\right) \times 0.6, \tag{A2}$$

where T is the first model-level air temperature but bounded to 283–305 K. If over snow, then for snow-layer temperature adjustments, min $\Delta T_s(1 \text{ or } 2) = -2.0$ and max $\Delta T_s(1 \text{ or } 2) = 1.0$.

2) The soil moisture adjustment is calculated generally [conditions defined below in (A4) and (A5)] as

$$\Delta\eta_s(k) = \alpha(k)\Delta\mathrm{RH}_a, \tag{A3}$$

where $\Delta\mathrm{RH}_a$ is the analysis increment of atmosphere relative humidity (calculated from temperature and water-vapor mixing ratio background and analyzed fields) at the lowest model level. The $\Delta\eta_s(k)$ is the soil volumetric water content (range 0–1; Smirnova et al. 1997) adjustment value in $\mathrm{m}^3\,\mathrm{m}^{-3}$ at kth soil

level. The $\alpha(k)$ is the adjustment factor for kth soil level. The factors for current applications in RAP–HRRR are listed in Table A2.

For nine-level soil model configuration, we allow adjustment to the top four levels. For the six-level soil model configuration, we only adjust the top two levels. The soil moistening (only) applied for the condition with $\Delta T_a < -0.15$ K is set as

$$\Delta\eta_s(k) = \begin{cases} 0.0, & \text{if} \quad \Delta\eta_s(k) < 0.0 \\ \alpha(k)\Delta \mathrm{RH}_a & \\ 0.03, & \text{if} \quad \Delta\eta_s(k) > 0.03 \end{cases}, \tag{A4}$$

where ΔT_a is the atmosphere temperature analysis increment in K at the lowest model level. Soil drying (applied for $\Delta T_a > 0.15$ K) is set as

$$\Delta\eta_s(k) = \begin{cases} 0.0, & \text{if} \quad \Delta\eta_s(k) > 0.0 \\ \alpha(k)\Delta \mathrm{RH}_a & \\ -0.03, & \text{if} \quad \Delta\eta_s(k) < -0.03 \end{cases}, \tag{A5}$$

where $\Delta \mathrm{RH}_a$ in its application to soil moisture adjustment is limited to -0.15 to 0.15. To avoid drying the soil too much, $\Delta \mathrm{RH}_a$ is limited further by

$$\Delta \mathrm{RH}_a = \Delta \mathrm{RH}_a \frac{\mathrm{RH}_a}{0.4} \quad \text{when}$$
$$\Delta \mathrm{RH}_a < 0.0 \quad \text{and} \quad \mathrm{RH}_a < 40\%, \tag{A6}$$

where RH_a is the analyzed atmosphere relative humidity at the lowest model level.

APPENDIX B

Description of Modifications to MYNN Boundary Layer Scheme

The version of the Mellor–Yamada–Nakanishi–Niino planetary boundary layer (PBL) scheme (MYNN) used in the Rapid Refresh deviates from the original form documented in Nakanishi and Niino (2004, 2009). The original version exhibited problems associated with the production of negative turbulent kinetic energy (TKE) and an inappropriate formulation of the turbulent mixing length within the PBL and free atmosphere. Also, the original scheme did not have a PBL height (z_i) diagnostic—a variable often required by other parameterization schemes available in ARW (e.g., shallow cumulus, chemical–/aerosol diffusion). Furthermore, ARW (prev3.7) lacked an option to couple parameterized shallow-cumulus clouds with the radiation scheme. Recent MYNN modifications to improve these deficiencies are described below, all of which are implemented in RAPv3.

a. *Modifications to prevent negative TKE*

Kitamura (2010) introduced a simple modification to the MYNN based on the method proposed by Canuto et al. (2008). Hereafter, this modification will be known as the Canuto–Kitamura (CK) modification. The CK modification applies a stability-dependent relaxation to the closure constant A_2, such that is no longer a constant in statically stable conditions (Ri > 0):

$$A_2 = \frac{A_2}{1 + \mathrm{MAX}(\mathrm{Ri}, 0.0)}. \tag{B1}$$

In the MYNN, the mixing length for vertical heat transport is given as $A_2 l_m$ (where l_m is the mixing length). Hence, this reformulation of A_2 causes the mixing length used for the turbulent heat flux to decrease with stronger static stability but does not affect the turbulent mixing of momentum. This modification was shown by Kitamura (2010) to remove the critical Richardson number (Ri_c), allowing small finite mixing to exist at $\mathrm{Ri} \to \infty$, as argued for by various turbulence researchers (i.e., Galperin et al. 2007; Zilitinkevich et al. 2007; Canuto et al. 2008).

Kitamura (2010) cautioned that CK modification may require subsequent adjustments to reduce the closure constants C_2 and C_3. We revised C_2 and C_3 to 0.729 and 0.34, respectively, within the range suggested by Gambo (1978); however, test simulations revealed that the removal of Ri_c encouraged excessive diffusivity in stable conditions, spurring efforts to further reduce the mixing-length scales as described below.

b. *Modifications to improve the mixing-length formulation*

The mixing-length reformulation is intended to 1) to reduce the scheme's diffusivity to earlier-version magnitudes and 2) improve turbulence representation in the free atmosphere. The MYNN mixing length l_m was designed such that the shortest length scale among the surface-layer length (l_s), turbulent length (l_t), and buoyancy length (l_b) will dominate:

$$\frac{1}{l_m} = \frac{1}{l_s} + \frac{1}{l_t} + \frac{1}{l_b}. \tag{B2}$$

The surface-layer length scale l_s, taken from Nakanishi (2001), is a function of the stability parameter ($\zeta = z/L$), where L is the Obukhov length ($= -u^3\theta_{v0}/kg\langle w'\theta_v'\rangle$; angle brackets indicate ensemble averages):

$$l_s = \begin{cases} kz/3.7 & \varsigma \geq 1 \\ kz(1 + c\varsigma)^{-1} & 0 \leq \varsigma < 1 \\ kz(1 - \alpha_4 \varsigma)^{0.2} & \varsigma < 0 \end{cases}, \quad \text{(B3)}$$

where z is the height AGL, k is the von Kármán constant (=0.4), and c and α_4 are chosen as 2.7 and 100, respectively. We reduce α_4 to 20 in order to reduce the near-surface turbulent mixing.

The form of the turbulent length scale l_t is taken from Mellor and Yamada (1974, 1982):

$$l_t = \alpha_1 \frac{\int_0^\infty qz\, dz}{\int_0^\infty z\, dz}, \quad \text{(B4)}$$

where $q = (\text{TKE})^{1/2}$ and α_1 is taken as 0.23 in Nakanishi and Niino (2004) as opposed to 0.10 in Mellor and Yamada (1974, 1982). Note that in (A4), the upper limit of integration makes l_t responsive to TKE anywhere in the grid column, perhaps far above the PBL. This limit was changed to $z_i + \Delta z$, where $\Delta z = 0.3 z_i$ is the transition-layer depth (Garratt 1992). With this modification, an accurate calculation of z_i becomes necessary (described below).

The buoyancy length scale l_b is given by

$$l_b = \begin{cases} \alpha_2 \dfrac{q}{N} & N > 0 \quad \text{and} \quad \varsigma \geq 0 \\ \dfrac{q}{N}\left[\alpha_2 + \dfrac{5}{\alpha_2}\left(q_c/l_t N\right)^{1/2}\right] & N > 0 \quad \text{and} \quad \varsigma < 0 \\ \infty & N \leq 0, \end{cases} \quad \text{(B5)}$$

where the Brunt–Väisälä frequency, $N = [(g/\theta_0)\partial\theta_v/\partial z]^{1/2}$ and $q_c = [(g/\theta_0)\langle w\theta_v\rangle_g l_t]^{1/3}$, is a turbulent-velocity scale. The coefficient α_2 is important for modulating the size of l_b. Reducing α_2 from 1.0 to 0.60 is sufficient to help reduce the diffusivity to typical values seen prior to the CK modification.

To improve the specification of free-atmosphere mixing lengths, a nonlocal formulation from Bougeault and Lacarrere (1989) was implemented. To largely restrict the use of the Bougeault–Lacarrere mixing length l_{BL} to the free atmosphere, a blending approach is adopted across the transition layer, where the averaged length scale l_m is used below z_i, and l_{BL} is used above.

c. Addition of the hybrid z_i diagnostic

The modifications presented above require the MYNN to use z_i as an internal variable. Results from Lemone et al. (2013, 2014) show that a potential-temperature-based definition of z_i is generally accurate for convective boundary layers, while TKE-based definitions are superior for stable boundary layers; therefore, a hybrid definition has been implemented. The potential-temperature-based definition of z_i ($z_{i,\theta}$) is taken from Nielsen-Gammon et al. (2008). The TKE-based definition of z_i ($z_{i,\text{TKE}}$) is taken to be the height at which the TKE decreases to below a threshold value, TKE_{min}. The quantity TKE_{min} was chosen to be 5% of the maximum near-surface TKE—a criterion also used by Kosović and Curry (2000). These two z_i definitions are blended such that $z_{i,\theta}$ will dominate for neutral and unstable conditions ($z_{i,\theta} > 200$ m), while $z_{i,\text{TKE}}$ will dominate for stable conditions ($z_{i,\theta} < 200$ m) using a transition-layer depth of 300 m. This hybrid algorithm has been shown to accurately diagnose the boundary layer height throughout a diurnal cycle (Fitch et al. 2013).

d. Coupling the subgrid-scale clouds from the MYNN to the radiation scheme

The MYNN employs a partial-condensation scheme to represent unresolved clouds. The presence of clouds contributes to a buoyancy flux that affects the production of TKE and the MYNN stability functions. The original MYNN uses the partial-condensation scheme of Sommeria and Deardorff (1977) to estimate the subgrid-scale cloud fraction and mixing ratio, but this scheme has been found to poorly represent shallow-cumulus coverage. The partial-condensation scheme was modified to use a relative-humidity (RH)-based cloud fraction, similar to Slingo (1980), but made dependent on the surface sensible heat flux. The cloud fraction (σ) is given by

$$\sigma = \left(\frac{\text{RH} - \text{RH}_c}{1 - \text{RH}_c}\right)^m, \quad \text{(B6)}$$

where $m = 2.0$ and the critical relative humidity RH_c is

$$\text{RH}_c = 1 - 0.35\left(1 - \frac{\text{HFX}_{\text{conv}} - \text{HFX}}{\text{HFX}_{\text{conv}}}\right)^2, \quad \text{(B7)}$$

where $\text{HFX}_{\text{conv}} = 250\ \text{W m}^{-2}$ and the surface sensible heat flux HFX is bounded between zero and HFX_{conv}. This form produces nonzero cloud fractions when RH > 65% and HFX > 250 W m^{-2}. Since this is only reasonable in shallow-cumulus environments, cloud fractions are only permitted in a layer between z_i and $z_i + \Delta z_{\text{shcu}}$. The depth of the layer, Δz_{shcu}, is a function of the mean RH in the boundary layer (RH_{PBL}) and HFX, suggested by Zhang and Klein (2013; but not given in functional form):

$$\Delta z_{\mathrm{shcu}}(\mathrm{m}) = 200 + \alpha_{\mathrm{HFX}}(\mathrm{RH}_{\mathrm{PBL}} + 0.5)^{1.5}, \quad \text{(B8)}$$

where $\alpha_{\mathrm{HFX}} = 3 \times \mathrm{MAX}(\mathrm{HFX}, 0.0)$. Thus, for strongly convective boundary layers ($\mathrm{HFX} > 500\,\mathrm{W\,m^{-2}}$) and $\mathrm{RH}_{\mathrm{PBL}} > 0.5$, the cloud layer Δz_{shcu} can exceed 1500 m, but in more moderate convective boundary layers, Δz_{shcu} ranges from 500 to 1500 m. The subgrid cloud fraction and subgrid-scale cloud water mixing ratio in the MYNN scheme are coupled to the radiation scheme in RAPv3.

e. *Evaluation of MYNN modifications with RAP*

Figure B1 shows diurnal composites of 12-h forecast biases and RMS errors for 2-m temperature and 10-m wind. Forecasts from RAPv3 (which uses the enhanced MYNN scheme) are compared with those from an experimental RAP without the MYNN enhancements described in this appendix. Improvements from the MYNN enhancements are evident in the wind speed biases and RMSEs throughout the diurnal cycle. The temperature bias and RMSE in RAPv3 are improved or comparable with those in the retracted-MYNN RAP except for a small degradation in the temperature RMSE from 1300 to 2000 UTC. A more detailed analysis will be presented in a forthcoming manuscript on MYNN development.

REFERENCES

Anthes, R. A., and D. P. Baumhefner, 1984: A diagram depicting forecast skill and predictability. *Bull. Amer. Meteor. Soc.*, **65**, 701–703.

Benjamin, S. G., and Coauthors, 2004a: An hourly assimilation/forecast cycle: The RUC. *Mon. Wea. Rev.*, **132**, 495–518, doi:10.1175/1520-0493(2004)132<0495:AHACTR>2.0.CO;2.

——, J. M. Brown, S. S. Weygandt, T. L. Smith, B. Schwartz, and W. R. Moninger, 2004b: Assimilation of surface cloud, visibility, and current weather observations in the RUC. *20th Conf. on Weather Analysis and Forecasting/16th Conf. on Numerical Weather Prediction*, Seattle, WA, Amer. Meteor. Soc., P1.47. [Available online at https://ams.confex.com/ams/84Annual/techprogram/paper_71242.htm.]

——, G. A. Grell, J. M. Brown, T. G. Smirnova, and R. Bleck, 2004c: Mesoscale weather prediction with the RUC hybrid isentropic/terrain-following coordinate model. *Mon. Wea. Rev.*, **132**, 473–494, doi:10.1175/1520-0493(2004)132<0473:MWPWTR>2.0.CO;2.

——, S. S. Weygandt, D. Dévényi, J. M. Brown, G. A. Manikin, T. L. Smith, and T. G. Smirnova, 2004d: Improved moisture and PBL initialization in the RUC using METAR data. *22nd Conf. on Severe Local Storms*, Hyannis, MA, Amer. Meteor. Soc., 17.3. [Available online at https://ams.confex.com/ams/11aram22sls/techprogram/paper_82023.htm.]

——, ——, S. E. Koch, and J. M. Brown, 2006: Assimilation of lightning data into RUC model forecasting. *Second Conf. on Meteorological Applications of Lightning Data*, Atlanta, GA, Amer. Meteor. Soc., 4.3. [Available online at https://ams.confex.com/ams/Annual2006/techprogram/paper_105079.htm.]

——, B. D. Jamison, W. R. Moninger, S. R. Sahm, B. E. Schwartz, and T. W. Schlatter, 2010: Relative short-range forecast impact from aircraft, profiler, radiosonde, VAD, GPS-PW, METAR, and mesonet observations via the RUC hourly assimilation cycle. *Mon. Wea. Rev.*, **138**, 1319–1343, doi:10.1175/2009MWR3097.1.

——, J. M. Brown, and T. G. Smirnova, 2016: Explicit precipitation-type diagnosis from a model using a mixed-phase bulk cloud-precipitation microphysics parameterization. *Wea. Forecasting*, doi:10.1175/WAF-D-15-0136.1, in press.

Bougeault, P., and P. Lacarrere, 1989: Parameterization of orography-induced turbulence in a mesobeta-scale model. *Mon. Wea. Rev.*, **117**, 1872–1890, doi:10.1175/1520-0493(1989)117<1872:POOITI>2.0.CO;2.

Canuto, V. M., Y. Cheng, A. M. Howard, and I. N. Easu, 2008: Stably stratified flows: A model with no Ri(cr). *J. Atmos. Sci.*, **65**, 2437–2447, doi:10.1175/2007JAS2470.1.

Cooper, W. A., 1986: Ice initiation in natural clouds. *Precipitation Enhancement—A Scientific Challenge*, *Meteor. Monogr.*, No. 43, Amer. Meteor. Soc., 29–32, doi:10.1175/0065-9401-21.43.29.

Fitch, A. C., J. K. Lundquist, and J. B. Olson, 2013: Mesoscale influences of wind farms throughout a diurnal cycle. *Mon. Wea. Rev.*, **141**, 2173–2198, doi:10.1175/MWR-D-12-00185.1.

Galperin, B., S. Sukoriansky, and P. S. Anderson, 2007: On the critical Richardson number in stably stratified turbulence. *Atmos. Sci. Lett.*, **8**, 65–69, doi:10.1002/asl.153.

Gambo, K., 1978: Notes on the turbulence closure model for atmospheric boundary layers. *J. Meteor. Soc. Japan*, **56**, 466–480.

Garratt, J. R., 1992: *The Atmospheric Boundary Layer*. Cambridge University Press, 316 pp.

Ghirardelli, J. E., and B. Glahn, 2010: The Meteorological Development Laboratory's aviation weather prediction system. *Wea. Forecasting*, **25**, 1027–1051, doi:10.1175/2010WAF2222312.1.

——, J. P. Charba, J.-S. Im, F. G. Samplatsky, B. Glahn, R. Yang, and A. J. Kochenash, 2015: Improving Localized Aviation MOS Program (LAMP) guidance by utilizing emerging forecast and observation resources. *Special Symp. on Model Post-Processing and Downscaling*, Phoenix, AZ, Amer. Meteor. Soc., 3.2. [Available online at http://www.nws.noaa.gov/mdl/lamp/publications/AMS_glmp_newdatasets_ghirardelli_etal_2015_final.pdf.]

Glahn, B., A. D. Schnapp, and J.-S. Im, 2015: The LAMP and HRRR ceiling height and visibility meld. NOAA/NWS MDL Office Note 15-1, 28 pp. [http://www.nws.noaa.gov/mdl/lamp/publications/lamp_hrrr_office_note_ON_15-1_7_31_15_final.pdf.]

Grell, G. A., and D. Devenyi, 2002: A generalized approach to parameterizing convection combining ensemble and data assimilation techniques. *Geophys. Res. Lett.*, **29**, 2002, doi:10.1029/2002GL015311.

——, and S. Freitas, 2014: A scale and aerosol aware stochastic convective parameterization for weather and air quality modeling. *Atmos. Chem. Phys.*, **14**, 5233–5250, doi:10.5194/acp-14-5233-2014.

——, S. E. Peckham, R. Schmitz, S. A. McKeen, G. Frost, W. C. Skamarock, and B. Eder, 2005: Fully coupled "online" chemistry in the WRF model. *Atmos. Environ.*, **39**, 6957–6976, doi:10.1016/j.atmosenv.2005.04.027.

Hamill, T. M., and C. Snyder, 2000: A hybrid ensemble Kalman filter–3D variational analysis scheme. *Mon. Wea. Rev.*, **128**, 2905–2919, doi:10.1175/1520-0493(2000)128<2905:AHEKFV>2.0.CO;2.

Iacono, M. J., J. S. Delamere, E. J. Mlawer, M. W. Shephard, S. A. Clough, and W. D. Collins, 2008: Radiative forcing by long-lived greenhouse gases: Calculations with the AER radiative transfer models. *J. Geophys. Res.*, **113**, D13103, doi:10.1029/2008JD009944.

Jacobs, A. J. M., and N. Maat, 2005: Persistence forecasting reference for aviation forecasts: Numerical guidance methods for decision support in aviation meteorological forecasting. *Wea. Forecasting*, **20**, 82–100, doi:10.1175/WAF-827.1.

Janjić, Z. I., 1994: The step-mountain eta coordinate model: Further developments of the convection, viscous sublayer, and turbulence closure schemes. *Mon. Wea. Rev.*, **122**, 927–945, doi:10.1175/1520-0493(1994)122<0927:TSMECM>2.0.CO;2.

——, 2002: Nonsingular implementation of the Mellor-Yamada Level 2.5 scheme in the NCEP meso model. National Centers for Environmental Prediction Office Note 437, 61 pp.

——, and R. L. Gall, 2012: Scientific documentation of the NCEP nonhydrostatic multiscale model on the B grid (NMMB). Part 1 dynamics. NCAR Tech. Note NCAR/TN-489+STR, 75 pp., doi:10.5065/D6WH2MZX.

Jeannot, E., 2000: Situation awareness—Synthesis of literature search. Eurocontrol Experimental Centre Note 16/00, 45 pp. [Available online at http://www.eurocontrol.int/eec/gallery/content/public/document/eec/report/2000/031_Situation_Awareness_Literature_Search.pdf.]

Kitamura, Y., 2010: Modifications to the Mellor-Yamada-Nakanishi-Niino (MYNN) model for the stable stratification case. *J. Meteor. Soc. Japan*, **88**, 857–864, doi:10.2151/jmsj.2010-506.

Kleist, D. T., D. F. Parrish, J. C. Derber, R. Treadon, W.-S. Wu, and S. Lord, 2009: Introduction of the GSI into the NCEP global data assimilation system. *Wea. Forecasting*, **24**, 1691–1705, doi:10.1175/2009WAF2222201.1.

Klemp, J. B., J. Dudhia, and A. D. Hassiotis, 2008: An upper gravity-wave absorbing layer for NWP applications. *Mon. Wea. Rev.*, **136**, 3987–4004, doi:10.1175/2008MWR2596.1.

Kosović, B., and J. A. Curry, 2000: A large eddy simulation study of a quasi-steady, stably stratified atmospheric boundary layer. *J. Atmos. Sci.*, **57**, 1052–1068, doi:10.1175/1520-0469(2000)057<1052:ALESSO>2.0.CO;2.

Lemone, M. A., M. Tewari, F. Chen, and J. Dudhia, 2013: Objectively determined fair-weather CBL depths in the ARW-WRF model and their comparison to CASES-97 observations. *Mon. Wea. Rev.*, **141**, 30–54, doi:10.1175/MWR-D-12-00106.1.

——, ——, ——, and ——, 2014: Objectively determined fair-weather NBL features in ARW-WRF and their comparison to CASES-97 observations. *Mon. Wea. Rev.*, **142**, 2709–2732, doi:10.1175/MWR-D-13-00358.1.

Mass, C., 2012: Nowcasting: The promise of new technologies of communication, modeling, and observations. *Bull. Amer. Meteor. Soc.*, **93**, 797–809, doi:10.1175/BAMS-D-11-00153.1.

Mellor, G. L., and T. Yamada, 1974: A hierarchy of turbulence closure models for planetary boundary layers. *J. Atmos. Sci.*, **31**, 1791–1806, doi:10.1175/1520-0469(1974)031<1791:AHOTCM>2.0.CO;2.

——, and ——, 1982: Development of a turbulence closure model for geophysical fluid problems. *Rev. Geophys. Space Phys.*, **20**, 851–875, doi:10.1029/RG020i004p00851.

Mittermaier, M., 2008: The potential impact of using persistence as a reference forecast on perceived forecast skill. *Wea. Forecasting*, **23**, 1022–1031, doi:10.1175/2008WAF2007037.1.

Nakanishi, M., 2001: Improvement of Mellor–Yamada turbulence closure model based on large-eddy simulation data. *Bound.-Layer Meteor.*, **99**, 349–378, doi:10.1023/A:1018915827400.

——, and H. Niino, 2004: An improved Mellor–Yamada level-3 model with condensation physics: Its design and verification. *Bound.-Layer Meteor.*, **112**, 1–31, doi:10.1023/B:BOUN.0000020164.04146.98.

——, and ——, 2009: Development of an improved turbulence closure model for the atmospheric boundary layer. *J. Meteor. Soc. Japan*, **87**, 895–912, doi:10.2151/jmsj.87.895.

NCEP, 2003: The GFS atmospheric model. NCEP Office Note 442, 14 pp. [Available online at http://www.emc.ncep.noaa.gov/officenotes/newernotes/on442.pdf.]

Nielsen-Gammon, J. W., and Coauthors, 2008: Multisensor estimation of mixing heights over a coastal city. *J. Appl. Meteor. Climatol.*, **47**, 27–43, doi:10.1175/2007JAMC1503.1.

Peckham, S. E., T. G. Smirnova, S. G. Benjamin, J. M. Brown, and J. S. Kenyon, 2016: Implementation of a digital filter initialization in the WRF Model and Its application in the Rapid Refresh. *Mon. Wea. Rev.*, **144**, 99–106, doi:10.1175/MWR-D-15-0219.1.

Phillips, N. A., 1957: A coordinate system having some special advantages for numerical forecasting. *J. Meteor.*, **14**, 184–185, doi:10.1175/1520-0469(1957)014<0184:ACSHSS>2.0.CO;2.

Skamarock, W. C., and Coauthors, 2008: A description of the Advanced Research WRF version 3. NCAR Tech. Note NCAR/TN-475+STR, 113 pp. [Available online at http://www2.mmm.ucar.edu/wrf/users/docs/arw_v3.pdf.]

Slingo, J. M., 1980: A cloud parameterization scheme derived from GATE data for use with a numerical model. *Quart. J. Roy. Meteor. Soc.*, **106**, 747–770, doi:10.1002/qj.49710645008.

Smirnova, T. G., J. M. Brown, and S. G. Benjamin, 1997: Evolution of soil moisture and temperature in the MAPS/RUC assimilation cycle. Preprints, *13th Conf. on Hydrology*, Long Beach, CA, Amer. Meteor. Soc., 172–175.

——, S. G. Benjamin, J. M. Brown, B. Schwartz, and D. Kim, 2000: Validation of long-term precipitation and evolved soil moisture and temperature fields in MAPS. *15th Conf. on Hydrology*, Long Beach, CA, Amer. Meteor. Soc., 1.15. [Available online at https://ams.confex.com/ams/annual2000/techprogram/paper_6846.htm.]

——, J. M. Brown, S. G. Benjamin, and J. S. Kenyon, 2016: Modifications to the Rapid Update Cycle Land Surface Model (RUC LSM) available in the Weather Research and Forecasting (WRF) Model. *Mon. Wea. Rev.*, doi:10.1175/MWR-D-15-0198.1, in press.

Smith, T. L., S. G. Benjamin, S. I. Gutman, and S. Sahm, 2007: Short-range forecast impact from assimilation of GPS-IPW observations into the Rapid Update Cycle. *Mon. Wea. Rev.*, **135**, 2914–2930, doi:10.1175/MWR3436.1.

——, ——, J. M. Brown, S. Weygandt, T. Smirnova, and B. Schwartz, 2008: Convection forecasts from the hourly updated, 3-km High Resolution Rapid Refresh (HRRR) model. *24th Conf. on Severe Local Storms*, Savannah, GA, Amer. Meteor. Soc., 11.1. [Available online at https://ams.confex.com/ams/24SLS/techprogram/paper_142055.htm.]

Sommeria, G., and J. W. Deardorff, 1977: Subgrid-scale condensation in models of nonprecipitating clouds. *J. Atmos.*

Sci., **34**, 344–355, doi:10.1175/1520-0469(1977)034<0344:SSCIMO>2.0.CO;2.

Thompson, G., and T. Eidhammer, 2014: A study of aerosol impacts on clouds and precipitation development in a large winter cyclone. *J. Atmos. Sci.*, **71**, 3636–3658, doi:10.1175/JAS-D-13-0305.1.

——, R. M. Rasmussen, and K. Manning, 2004: Explicit forecasts of winter precipitation using an improved bulk microphysics scheme. Part I: Description and sensitivity analysis. *Mon. Wea. Rev.*, **132**, 519–542, doi:10.1175/1520-0493(2004)132<0519:EFOWPU>2.0.CO;2.

——, P. R. Field, R. M. Rasmussen, and W. D. Hall, 2008: Explicit forecasts of winter precipitation using an improved bulk microphysics scheme. Part II: Implementation of a new snow parameterization. *Mon. Wea. Rev.*, **136**, 5095–5115, doi:10.1175/2008MWR2387.1.

Wang, X., 2010: Incorporating ensemble covariance in the gridpoint statistical interpolation variational minimization: A mathematical framework. *Mon. Wea. Rev.*, **138**, 2990–2995, doi:10.1175/2010MWR3245.1.

Weygandt, S. S., and S. Benjamin, 2007: Radar reflectivity-based initialization of precipitation systems using a diabatic digital filter within the Rapid Update Cycle. *22nd Conf. on Weather Analysis and Forecasting/18th Conf. on Numerical Weather Prediction*, Park City, UT, Amer. Meteor. Soc., 1B.7. [Available online at https://ams.confex.com/ams/22WAF18NWP/techprogram/paper_124540.htm.]

——, ——, T. G. Smirnova, and J. M. Brown, 2008: Assimilation of radar reflectivity data using a diabatic digital filter within the Rapid Update Cycle. *12th Conf. on IOAS-AOLS*, New Orleans, LA, Amer. Meteor. Soc., 8.4. [Available online at https://ams.confex.com/ams/88Annual/techprogram/paper_134081.htm.]

Whitaker, J. S., T. M. Hamill, X. Wei, Y. Song, and Z. Toth, 2008: Ensemble data assimilation with the NCEP Global Forecast System. *Mon. Wea. Rev.*, **136**, 463–48, doi:10.1175/2007MWR2018.1.

Wilczak, J., and Coauthors, 2015: The Wind Forecast Improvement Project (WFIP): A public–private partnership addressing wind energy forecast needs. *Bull. Amer. Meteor. Soc.*, **96**, 1699–1718, doi:10.1175/BAMS-D-14-00107.1.

WMO, 2015: USA AMDAR Programme—Smoothed monthly average of daily (aircraft) report totals. [Available online at http://www.wmo.int/pages/prog/www/GOS/ABO/data/statistics/aircraft_obs_cmc_mthly_ave_daily_reports_USA.jpg.]

Wu, W.-S., 2005: Background error for NCEP's GSI analysis in regional mode. *Proc. Fourth Int. Symp. on Assimilation of Observations in Meteorology and Oceanography*, Prague, Czech Republic, WMO, 3A.27.

——, R. J. Purser, and D. F. Parrish, 2002: Three-dimensional variational analysis with spatially inhomogeneous covariances. *Mon. Wea. Rev.*, **130**, 2905–2916, doi:10.1175/1520-0493(2002)130<2905:TDVAWS>2.0.CO;2.

Zhang, Y., and S. A. Klein, 2013: Factors controlling the vertical extent of fair-weather shallow cumulus clouds over land: Investigation of diurnal-cycle observations collected at the ARM Southern Great Plains site. *J. Atmos. Sci.*, **70**, 1297–1315, doi:10.1175/JAS-D-12-0131.1.

Zilitinkevich, S. S., T. Elperin, N. Kleeorin, and I. Rogachevskii, 2007: Energy- and flux-budget (EFB) turbulence closure model for stably stratified flows. Part I: Steady-state, homogeneous regimes. *Bound.-Layer Meteor.*, **125**, 167–191, doi:10.1007/s10546-007-9189-2.